AMOC and summer sea ice as key drivers of the spread in mid-holocene winter temperature patterns over Europe in PMIP3 models

Alina Găinuşă-Bogdan, Didier Swingedouw, Pascal Yiou, Julien Cattiaux, Francis Codron, Simon Michel

AMOC and summer sea ice as key drivers of the spread in Mid-Holocene winter temperature patterns over Europe in PMIP3 models

Alina Găinuşă-Bogdan[1,2], Didier Swingedouw[1], Pascal Yiou[2], Julien Cattiaux[3], Francis Codron[4] and Simon Michel[1]

[1] *Environnements et Paléoenvironnements Océaniques et Continentaux (EPOC), UMR CNRS 5805 EPOC—OASU—Université de Bordeaux, Allée Geoffroy Saint-Hilaire, Pessac 33615, France.*

[2] *Laboratoire des Sciences du Climat et de l'Environnement, UMR8212 CEA-CNRS-UVSQ, Institut Pierre Simon Laplace, Université Paris-Saclay, 91191 Gif-sur-Yvette, France*

[3] *Centre National de Recherches Météorologiques, Université de Toulouse, UMR 3589 CNRS/Météo-France, Toulouse, France.*

[4] *Sorbonne Université, CNRS, IRD, MNHN, Laboratoire d'Océanographie et du Climat (LOCEAN/IPSL), 4 place Jussieu, Paris F-75005, France.*

Contact: alina.gainusabogdan@gmail.com

Abstract

The mid-Holocene (6,000 years before present) was a warmer period than today in summer in most of the Northern Hemisphere. In winter, over Europe, pollen-based reconstructions show a dipole of temperature anomalies as compared to present-day, with warmer conditions in the north and colder in the south. It has been proposed that this pattern of temperature anomaly could be explained by a persisting positive phase of the North Atlantic Oscillation during this period, which was, however, not reproduced in general by climate models. Indeed, PMIP3 models show a large spread in their response to the mid-Holocene insolation changes, the physical origins of which are not understood. To improve the understanding of the

reconstructed temperature changes and of the PMIP3 model spread, we analyze the dynamical response of these model simulations in the North Atlantic for mid-Holocene conditions as compared to pre-industrial. We focus on the European pattern of temperature in winter and compare the simulations with a pollen-based reconstruction. We find that some of the model simulations yield a similar pattern to the reconstructed one, but with far lower amplitude, although it remains within the reconstruction uncertainty. We attribute the northern warm part of the latitudinal dipole of temperature anomaly in winter to a lower sea-ice cover in the Nordic Seas. The decrease of sea ice in winter indeed reduces the local sea-ice insulation effect, allowing the released ocean heat to reach continental northern Europe. This decrease in winter sea-ice cover is related to an increase in the Atlantic meridional overturning circulation (AMOC) and its associated ocean heat transport, as well as the effect of insolation changes on sea ice in summer, which persists until winter. We only find a slight cooling signal over southern Europe, compared to reconstructions, mainly related to the insolation-induced cooling in winter over Africa. We show that the models that failed to reproduce any AMOC increase under mid-Holocene conditions are also the ones that do not reproduce the temperature pattern over Europe. The change in sea level pressure is not sufficient to explain the spread among the models. The ocean-sea ice mechanisms that we proposed constitute an alternative explanation to the pattern of changes in winter temperatures over Europe in the mid-Holocene, which is in better agreement with available model simulations of this period. Finally, we evaluate if reconstructions of the AMOC for the mid-Holocene can provide interesting emerging constraints on key changes in European climate, and indirectly on AMOC response to on-going and future radiative changes. Although there is a significant link between the response of the mid-Holocene and projections, it remains limited. The proposed mechanism does not appear to be sufficient to explain the large discrepancies between models and reconstruction data for the summertime period.

Keywords: PMIP3, Mid-Holocene, NAO, AMOC, inter-model spread

Introduction

Projections of the climate of Europe show a large spread for the ongoing century (IPCC Working Group 1 et al. 2013). For a given emission scenario, uncertainties are related to the internal variability, that can be large at the regional scale (Deser et al. 2012), and to the model-dependent sensitivity of the climate system to external forcings (Hawkins and Sutton 2009). In particular, changes of the atmospheric or oceanic circulation tend to vary a lot between models. Future projections of the North Atlantic Oscillation (NAO), that plays a crucial role in the climate variability of Europe in winter (Hurrell 1995), do not even agree on its sign (Cattiaux and Cassou 2013). At multi-decadal timescales, the Atlantic Meridional Overturning Circulation (AMOC) also plays a key role for the climate of Europe through its massive northward transport of heat all along the Atlantic Ocean (Swingedouw et al. 2009, Haarsma et al. 2015, Jackson et al. 2015). Its long-term projections are, similarly, very uncertain (Weaver et al. 2012), even though all the models agree that it should decrease in the coming century, especially when the Greenland ice sheet melting is accounted for (Bakker et al. 2016; Swingedouw et al. 2015a). To improve our estimate of the response of the NAO or the AMOC to external forcing, paleoclimate data could provide key observational constraints (Schmidt et al. 2014; Harrison et al. 2015).

Paleoclimate reconstructions are based on proxy records that have been collected for decades around the world. The main issue with proxies is that they are indirect records of climate variables, so that they could be subject to large uncertainties and biases. Nevertheless, except for the short instrumental era, they are the only observational estimates of the climate response to different external forcings. Even though there is no exact analogue of the future in the past, information on the climate response to changes in external forcings has a high relevance to better evaluate the sensitivity of climate models and possibly reduce the

uncertainty concerning the on-going climate change (Schmidt et al. 2014), especially at the regional scale.

The mid-Holocene (MH: 6000 years Before Present) is a period for which reconstructions suggest a mean climate of the northern high latitudes that was considerably warmer than today in summer (Fischer et al. 2018), due to a different insolation forcing (Figure 1). This is an interesting climate period, when the Sahara is suspected to have been greener than today (Claussen and Gayler 1997). This is why the Paleoclimate Model Intercomparison Project, phase 3 (PMIP3) initiative (Braconnot et al. 2012) proposed this period as a key snapshot to be simulated by the same climate models that produce climate projections (Schmidt et al. 2014; Harrison et al. 2015).

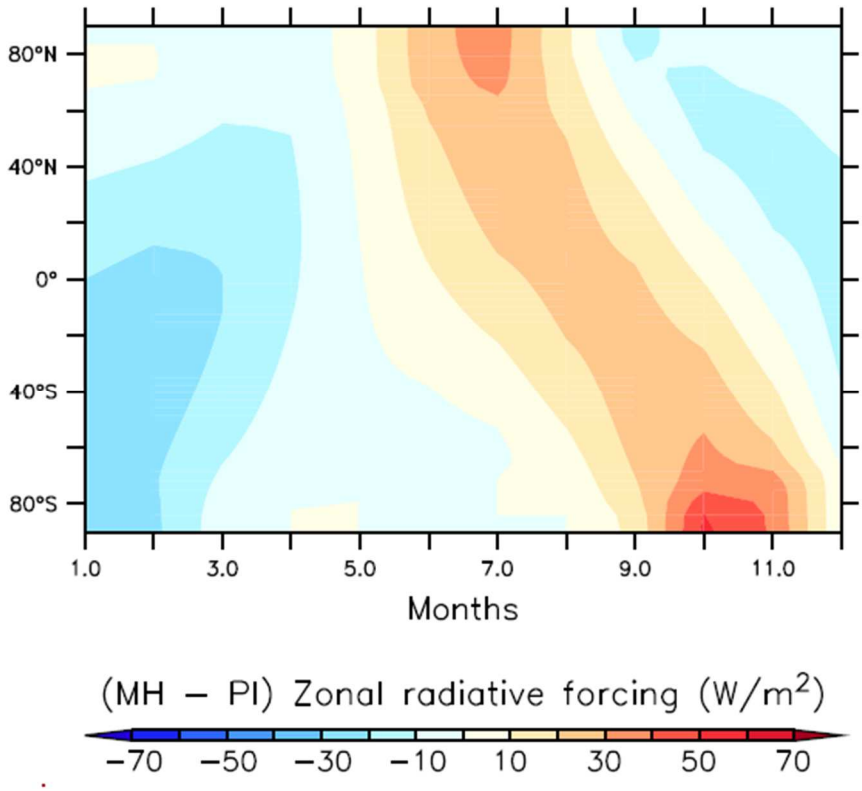

Figure 1: Zonally-averaged climatological monthly differences in the incoming shortwave radiation at the top of the atmosphere between mid-Holocene and pre-industrial simulations.

A recent study proposed an improved reconstruction of climate over Europe for the MH based on a broad compilation of pollen data (Mauri et al. 2014). The results showed a dipole of winter near-surface temperature anomalies, with warm anomalies in the north of Europe and cold anomalies in the south. The authors suggested this pattern could be caused by an atmospheric circulation anomaly similar to a positive phase of the North Atlantic Oscillation (NAO^+). Other studies also proposed such a change for mid-Holocene European climate in winter (Guyard et al. 2013; Chabaud et al. 2014). This hypothesis therefore provides an interesting testbed for climate models. Mauri et al. (2014) argued that PMIP3 simulations in general did not reproduce very well the reconstructed dipole in temperature in winter because they do not show any NAO^+-like changes in atmospheric circulation for the MH. This was also the case for the older PMIP2 dataset (Gladstone et al. 2005). Nevertheless, it has been proposed that PMIP2 dataset still showed some skill in capturing the pattern of climate change over Europe for the MH (Brewer et al. 2007). While the new generation of PMIP3 models show larger changes in sea ice for MH conditions than PMIP2 models over the Arctic (Berger et al. 2013), which may impact the response over Europe, a quantitative comparison of the PMIP3 models with winter reconstruction of temperature over Europe has not been made yet. Furthermore, a detailed analysis of the mechanism explaining the wintertime response in PMIP3 simulations for MH is also missing for the North Atlantic.

The large increase in summer insolation for MH conditions may have strongly affected the sea ice in polar regions, even in winter through inertia. This could then influence the continental climate, notably in winter where the heat flux release by the ocean is largest, as well as the insulation effect of sea ice (Goosse et al. 2002). Such an impact was illustrated by Fischer and Jungclaus (2011) in a transient simulation over part of the Holocene using the MPI climate model. Otto et al. (2009), using different simulations for the MH where the coupling between the ocean and vegetation was either activated or not, also showed that the ocean plays a key role for the amplitude of the temperature response of the northern high

latitudes to the radiative forcing. The insolation during the MH was indeed very different from the pre-industrial period. The latitudinal gradient was strongly reduced during the summer season, which could have impacted the oceanic and atmospheric meridional heat transport (Davis and Brewer 2009).

In the present study, we propose to analyze the response of climate models participating in PMIP3 under MH wintertime conditions, with a specific focus on the North Atlantic region. We will assess the potential causes for the model spread in temperature response over Europe in winter and analyze the role played by changes in atmospheric circulation, oceanic circulation and radiative changes amplified by sea ice response. We will also compare these simulations, using classical skill scores, with the reconstruction of Mauri et al. (2014). This will allow us to determine the models that best reproduce the temperature dipole pattern over Europe. Our main result is that atmospheric circulation changes are not the main driver of the simulated patterns of temperature anomalies. These are instead linked to sea-ice anomalies, forced either by AMOC slowdown or summer sea-ice melt.

Experimental design

We analyze pairs of mid-Holocene and pre-industrial (PI) simulations performed with PMIP3 climate models. Only 12 models (Table 1) are retained, as we require at least 100 years of both PI and MH simulations to perform robust statistical analyses. When more than 200 model years are available, we use the last 200 years of the simulation. Throughout the analyses, we use data on the native grid for each model, except when multi-model statistics are calculated, in which case the model data is first interpolated on a regular 1°x1° grid for the temperature to be compared with Mauri et al. (2014) and a regular 2.5°x2.5° grid for the other variables. We also use RCP85 projections of the AMOC for the CMIP5 models available in

139 order to compare the simulated changes in the AMOC in these projections to those for the
140 mid-Holocene.

Index	Model	Modeling Center	Reference
A	bcc-csm1-1	Beijing Climate Center (BCC)	Xin et al. (2013)
B	CNRM-CM5	Centre National de Recherches Météorologiques/ Centre Européen de Recherche et Formation Avancées en Calcul Scientifique (CNRM/CERFACS)	Voldoire et al. (2013)
C	CSIRO-Mk3-6-0	Commonwealth Scientific and Industrial Research Organization/ Queensland Climate Change Centre of Excellence (CSIRO-QCCCE)	Rotstayn et al. (2012)
D	IPSL-CM5A-LR	Institut Pierre-Simon Laplace (IPSL)	Dufresne et al. (Dufresne et al. 2013)
E	FGOALS-g2	State Key Laboratory of Numerical Modeling for Atmospheric Sciences and Geophysical Fluid Dynamics/Institute of Atmospheric Physics (LASG/IAP)	Li et al. (2013)
F	FGOALS-s2	LASG/IAP	Bao et al. (2013)
G	MIROC-ESM	Atmosphere and Ocean Research Institute (The University of Tokyo), National Institute for Environmental Studies, and Japan Agency for Marine-Earth Science and Technology	Watanabe et al. (2011)
H	HadGEM2-ES	Met Office Hadley Center (MOHC)	Collins et al. (2011)
I	MPI-ESM	Max Planck Institute for Meteorology (MPI-M)	Jungclaus et al. (2013)
J	MRI-CGCM3	Meteorological Research Institute (MRI)	Yukimoto et al. (2012)
K	GISS-E2-R	NASA Goddard Institute for Space Studies	Schmidt et al. (2006)
L	CCSM4	National Center for Atmospheric Research (NCAR)	Gent et al. (2011)

141
142 **Table 1:** List of PMIP3 models included in this study.

143 We focus our analysis on Mid-Holocene climatological anomalies with respect to the pre-
144 industrial period for wintertime (December-February averages – DJF), summertime (June-
145 August averages – JJA) or annual means (ANM). Wherever suitable, we use a two-sided
146 independent sample t-test to determine if and to what level these anomalies are statistically
147 significant, considering the interannual variability in the PI and MH simulations, at each grid

point. Where this is done, we shade in color the regions where the anomalies are significant at the 90% confidence level. For a more stringent test, we add contours corresponding to significant anomalies at the 99% confidence interval.

Temperature and circulation response

MH winter temperature response in PMIP3 models

While the external forcing (insolation changes) is the same in the different models, their responses to MH climatic condition in winter over Europe are very different, as illustrated in Figure 2. This figure shows the significant winter surface atmospheric temperature (SAT) anomalies over Europe simulated with the 12 different climate models, the multi-model ensemble mean anomaly and the reconstruction by Mauri et al. (2014). The uncertainties in the pollen-based reconstruction can be quite large, therefore Figure 2n only shows those $\Delta SAT_{DJF,EU}$ values that are larger in absolute value than the respective estimated uncertainties. We find a wide range of simulated SAT anomaly patterns between the 12 models, and some important differences from the mean reconstructed pattern. We quantify these model-reconstruction differences in Figure 3, showing the pattern correlation, pattern root-mean-square difference (RMSE; pattern RMSE obtained by removing the respective spatial average from each field before the RMSE calculation) and full-field RMSE for each model compared to the Mauri et al. (2014) reconstruction, as well as for the multi-model ensemble mean.

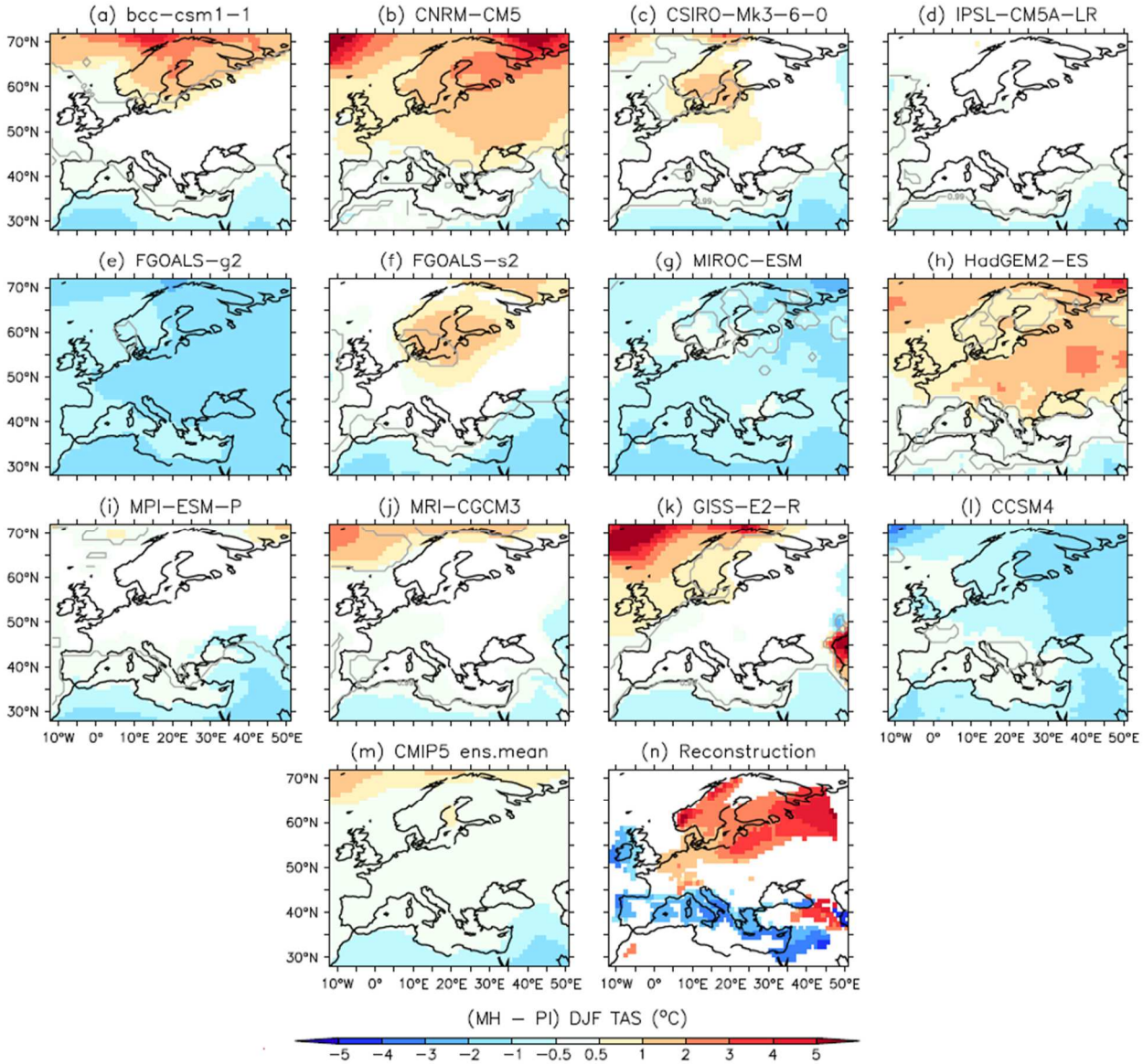

166
167 **Figure 2:** (a)-(l) Significant differences (color: at 90% confidence level; inside contours: at 99% confidence
168 level) between mean wintertime near-surface air temperature (SAT) in mid-Holocene and pre-industrial
169 simulations run with 12 different climate models; (m) Multi-model ensemble mean difference between MH and
170 PI climatological wintertime SAT; (n) Mauri et al. (2014) reconstruction of the MH climatological wintertime
171 SAT anomaly – only data where the signal is larger than the estimated uncertainty is considered.

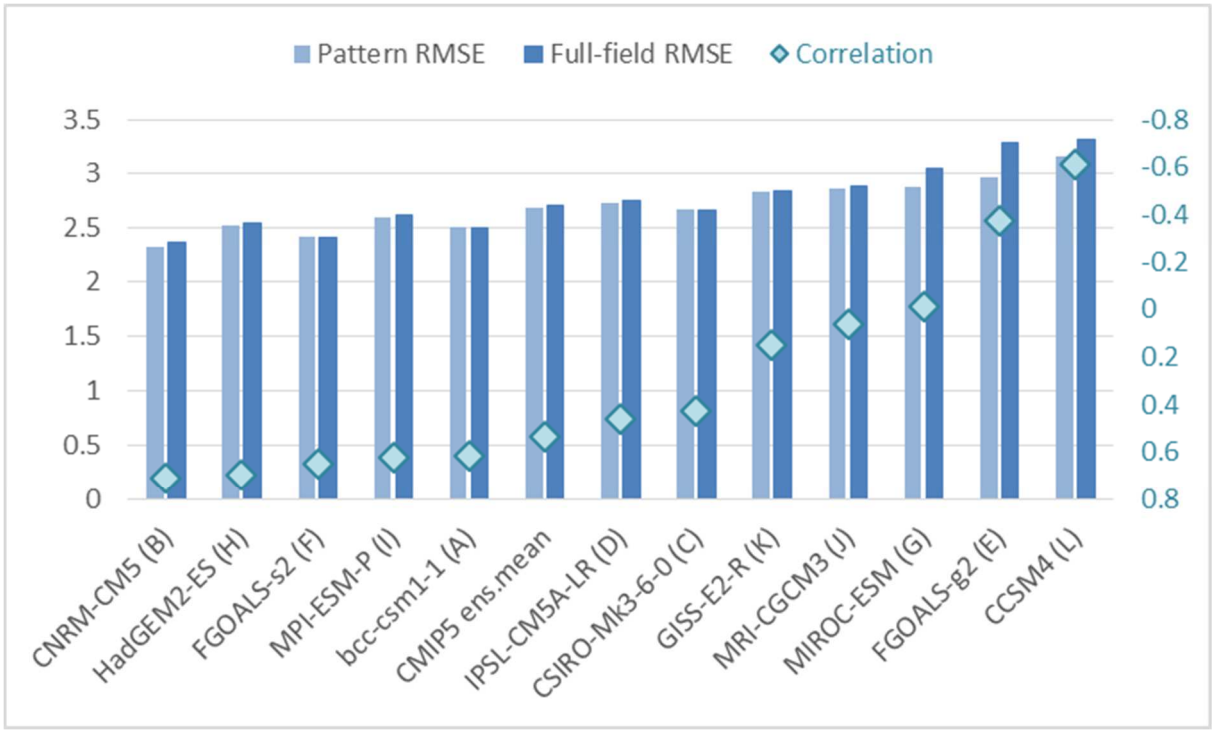

Figure 3: Statistics comparing the simulated and reconstructed (Mauri et al. 2014) mid-Holocene wintertime SAT anomalies over Europe. Correlation (values shown on the right-side vertical axis): spatial correlation coefficient between the two fields compared; Pattern RMSE: root-mean-square error when the respective spatial average has been removed from each of the two fields compared; Full-field RMSE: total root-mean-square-difference between the two fields. The model data, including the multi-model ensemble mean, are sorted from the highest to the lowest spatial correlation with the reconstructed data. The statistics are only calculated using those grid points where the reconstructed signal is stronger than the estimated uncertainty (see Figure 2n).

Some models fail to represent the reconstructed $\Delta SAT_{DJF, EU}$ pattern, like CCSM4, FGOALS-g2 and MIROC-ESM, which show near-zero or negative spatial correlation coefficients with the reconstructed field and RMSEs larger than 3°C. Other models like CNRM-CM5 and HadGEM2-ES have some success in simulating a similar pattern, *i.e.*, a positive north-south temperature anomaly gradient (spatial correlation coefficient ~0.7) but still fail at simulating the reconstructed amplitude (pattern RMSE $\geq$ 2.3°C), and the temperature anomalies themselves (full-field RMSE $\geq$ 2.4°C).

In terms of latitudinal gradient, Figure 4 shows the zonal mean anomalies of wintertime temperatures over continental Europe in the models compared to the reconstruction. This figure clearly shows that all the models do not reproduce the amplitude of the dipole between northern and southern Europe. It also shows that the uncertainty in the temperature reconstruction is large and there are three models that are within the error bar of the reconstruction for this diagnostic for more than 95% of the latitude range considered: CNRM-CM5, FGOALS-s2 and bcc-csm1-1. The first two are also in the top three for the RMSE and correlation (cf. Figure 3). This shows that some models succeed in reproducing the reconstruction latitudinal gradient when considering the uncertainty in the reconstruction, although with a lower amplitude as compared to the best guess. We also notice that the precise pattern is usually not perfectly reproduced (*e.g.* cooling signal over Ireland in the reconstruction).

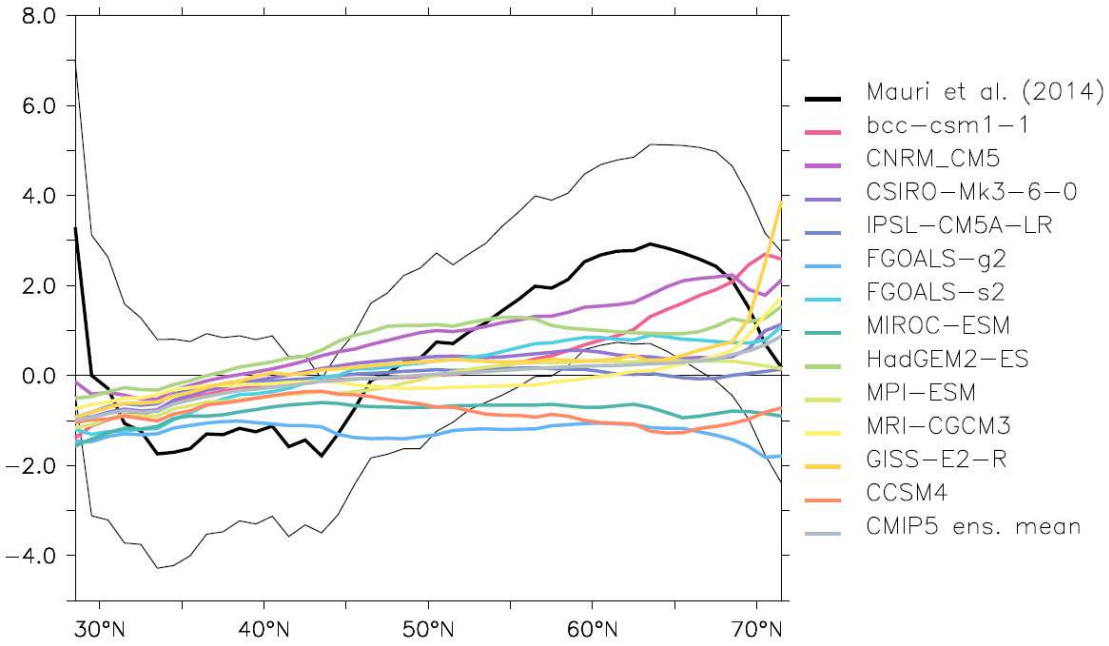

Figure 4: Zonal means of the climatological wintertime temperature anomalies over Europe – model results vs. Mauri et al. (2014) reconstruction. The reconstruction is shown in black (thick line) with its associated uncertainty (thin lines). The different models are shown in color and the model ensemble mean is shown in grey. All model data have been regridded onto the reconstruction data grid and the same (reconstruction) land-sea mask was applied before the calculation of the zonal means.

205

206 **MH winter atmospheric circulation anomalies in the PMIP3 models**

207 Mauri et al. (2014) proposed that the MH temperature anomaly pattern over Europe could be
208 caused by a NAO-like atmospheric circulation anomaly. To explore this possibility in the
209 PMIP3 database, Figure 5 shows the statistically significant sea-level pressure differences
210 (ΔSLP) between the climatological wintertime (DJF) MH and PI simulations over the North
211 Atlantic (NA) sector for the 12 analyzed models. All models show significant MH winter SLP
212 anomalies, of the order of 0.5-1.5 hPa, with corresponding 1000-hPa wind speed anomalies
213 ($\Delta U_{horiz,DJF,1000}$, not shown) of the order of 0.2-0.7 m/s.

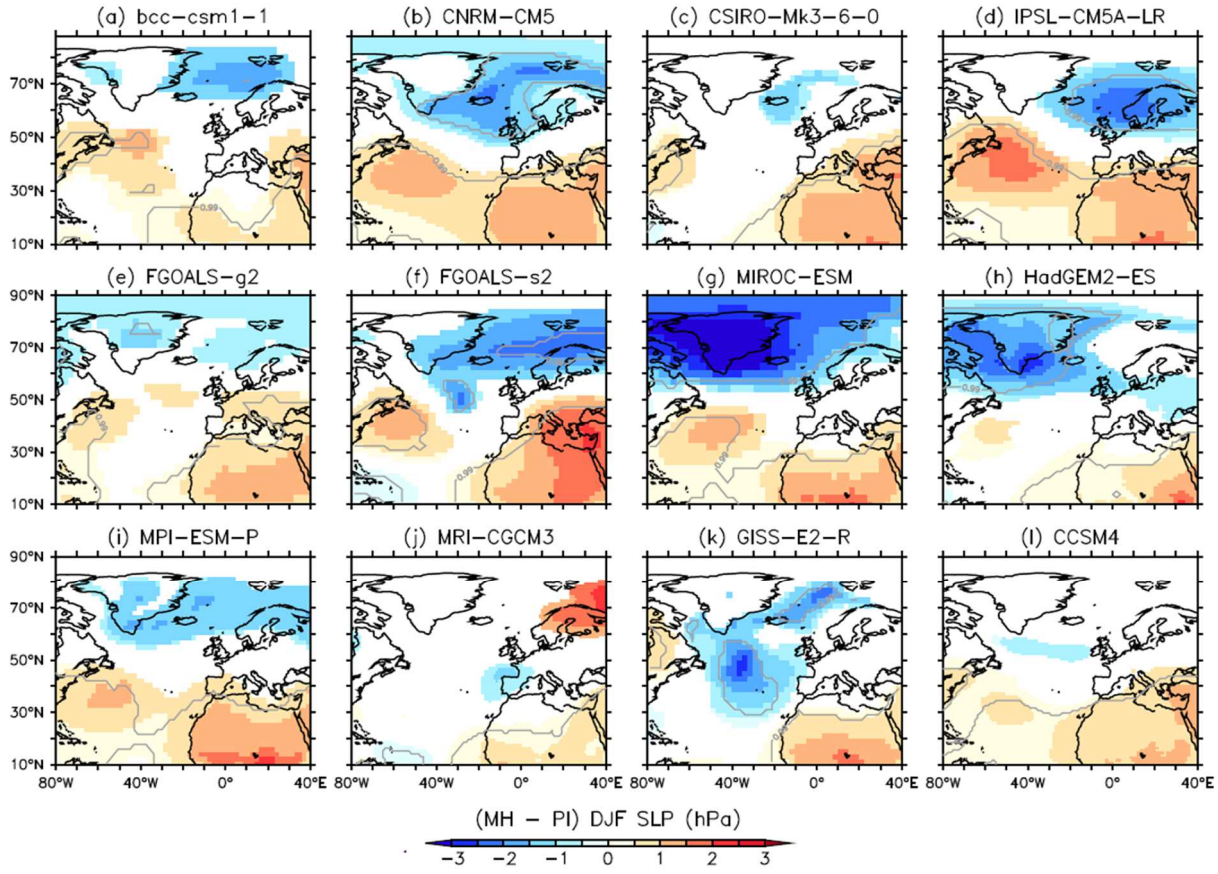

214

215 **Figure 5**: Significant differences (color: at 90% confidence level; inside contours: at 99% confidence
216 level) between mean wintertime sea-level pressure in mid-Holocene and pre-industrial simulations run
217 with 12 different climate models.

Figure 6 shows the multi-model mean circulation anomalies at different levels in the troposphere. Significant anomalies (two-sided independent sample t-test of significance of the MH-PI difference using the last 200 years of each simulation or, where simulations were shorter, all years of the simulations) at the 99% level are found at all atmospheric levels. The most notable feature is a negative zonal wind speed anomaly in the subtropics (around 30^{o}N), maximum at upper levels (Δu_{200}) and over the western half of the North Atlantic. This feature is present and prominent in all models (with the exception of GISS-E2-R where the significant anomaly is present, but much weaker than in the other models, not shown), but with structures varying in strength, extent and zonal orientation. We can trace it to a local weakening of the jet streams (in some models, accompanied by a slight northward shift of the eddy-driven jet) and, for most models, a more marked separation between the eddy-driven and subtropical jet streams over the North Atlantic (illustrated in Figure 6a for the multi-model ensemble mean). This results in an anticyclonic horizontal wind speed anomaly and local high pressure in the West Atlantic northward of the negative Δu_{200} region. For most models, this anticyclonic anomaly dominates the pattern of mean atmospheric circulation change over the North Atlantic. In those cases, this anomaly structure is found throughout the atmospheric column (as illustrated in Figures 6b and 6c for the 500 hPa level), down to the surface (Figure 6e), explaining the positive SLP anomalies found in most models over the southwestern North Atlantic (Figure 5, Figure 6d). Even the MRI model, which has no significant anomalies in the lower atmosphere, shows a similar significant anomaly in the jet stream (not shown).

While this positive pressure anomaly in the Western Atlantic has an equivalent barotropic structure that extends throughout the troposphere, the positive SLP anomaly seen over North Africa in the multi-model mean (Figure 6d) is on the contrary very shallow, disappearing or even changing sign at 500 hPa. This baroclinic structure is linked to a cold temperature anomaly in the atmospheric column, which can be explained by the negative DJF radiative

forcing. The reduction of the radiative forcing is strongest at low latitudes (Figure 1), and has a larger impact over continental regions like North Africa.

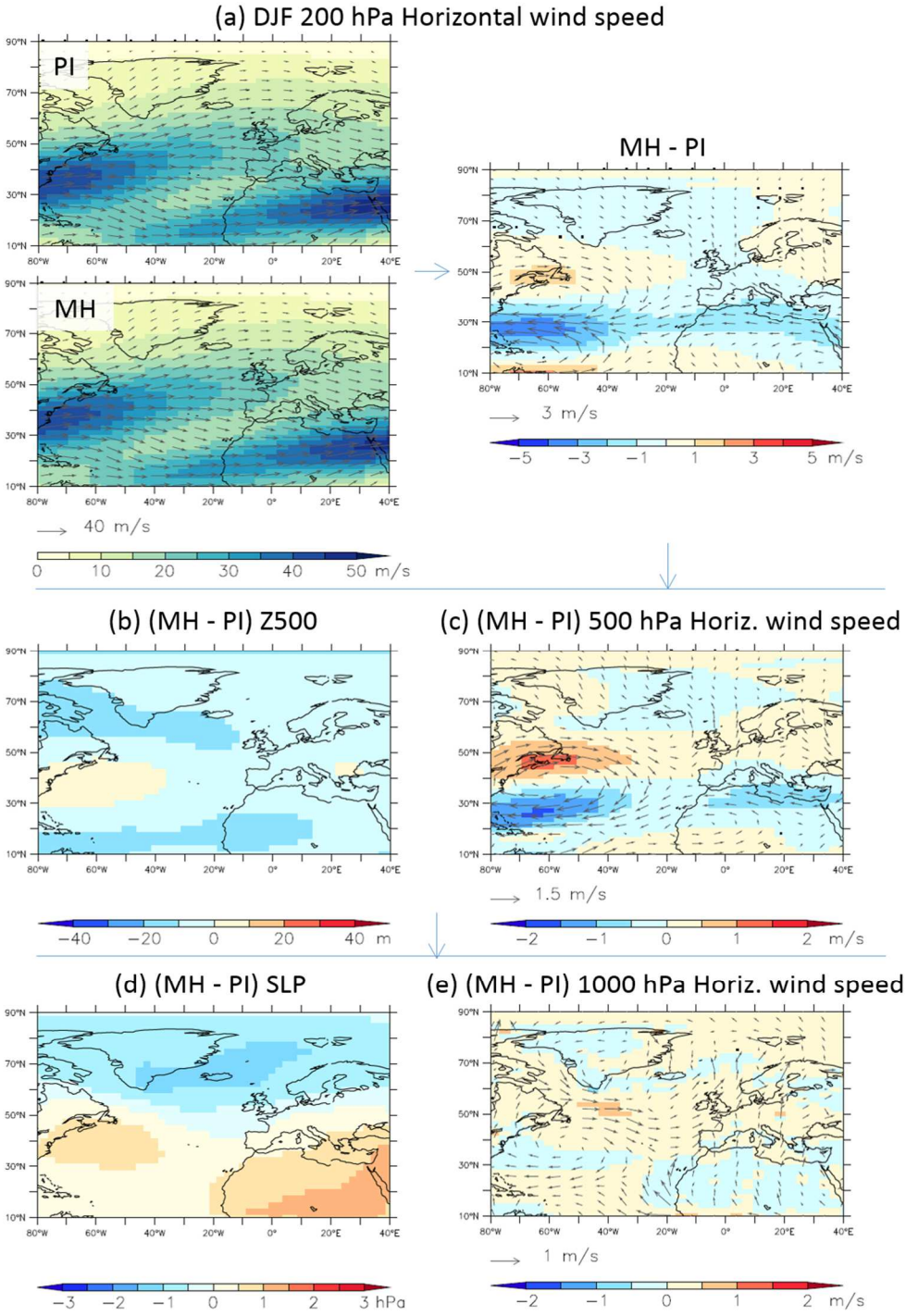

Figure 6: Multi-model ensemble mean wintertime: (a) 200 hPa horizontal wind speed in pre-industrial (PI), mid-Holocene (MH) simulations and the corresponding MH-PI difference; (b) 500 hPa geopotential height MH anomaly; (c) 500 hPa horizontal wind speed anomaly; (d) sea-level pressure anomaly; (e) 1000 hPa horizontal wind speed anomaly. We used a two-sided independent sample t-test of significance of the MH-PI differences

(based on the last 200 years or, where shorter, on the full time series of the MH and the PI simulations, respectively), for each model. For each model, we have found significant MH-PI differences at the 99% confidence level. The anomaly patterns were very similar from one model to the other, which allowed us to present the anomaly maps for the multi-model ensemble as representative of the ensemble of models.

Atmospheric circulation vs. European temperature anomaly patterns

Figure 5 shows that several PMIP3 models simulate a positive SLP anomaly over the southern part of the North Atlantic and a negative SLP anomaly over the northern part of the basin during MH winters. This pattern could be roughly construed to be NAO^+-like, as Mauri et al. (2014) argued could cause their reconstructed DJF ΔSAT_{EU} pattern. This section examines whether such a relationship between a NAO^+-like circulation anomaly and a ΔSAT_{EU} pattern can be found within our multi-model ensemble.

A key question is whether the differences between the simulated temperature anomaly patterns between models can be attributed to the differences in their simulated atmospheric circulation anomalies over the North Atlantic. More specifically, we want to assess whether the models that simulate a positive north-south temperature gradient over Europe are only the models that also simulate a NAO^+-like circulation anomaly over the North Atlantic.

A qualitative comparison of Figure 2 and Figure 5 indicates that this is not the case. While the hypothesis of a NAO^+-like cause of marked north-south gradients in $\Delta SAT_{DJF, EU}$ could hold for a few models (*e.g.*, CNRM-CM5), the ensemble of models does not support it. Some models exhibit a NAO^+-like circulation without a strong north-south $\Delta SAT_{DJF, EU}$ gradient (*e.g.*, IPSL-CM5A-LR, MIROC-ESM), while other models show a marked $\Delta SAT_{DJF, EU}$ gradient without simulating a NAO^+-like circulation anomaly (*e.g.*, GISS-E2-R). For some model simulations showing a negative SLP anomaly around Iceland, which can look like part of a NAO^+ pattern, just like over Africa the pressure anomaly disappears with height (not shown), and is most likely a thermal structure caused by the local warming at the surface.

For a quantitative assessment, Figure 7 evaluates the relationship between first-order indices of the large-scale temperature and circulation changes, namely the north-south $\Delta SAT_{DJF,\,EU}$ gradient and the NAO$^+$-like ΔSLP_{NA}. The north-south $\Delta SAT_{DJF,\,EU}$ gradient is defined as the mean temperature difference between a northern and a southern region over Europe chosen to approximately reflect the Arctic Oscillation signature on SAT_{EU}, as shown in Mauri et al. (2014) (top left panel in Figure 7 below). The NAO$^+$-like ΔSLP_{NA} is defined as the mean sea-level pressure difference between regions chosen to approximately reflect the centers of action of the North Atlantic Oscillation index (*cf.* Hurrell & Deser 2010 – bottom right panel in Figure 7). The scatterplot between the two indices in the top right panel of Figure 7 shows a lack of significant correlation that confirms that the PMIP3 models do not support a straightforward link between MH temperature anomaly patterns over Europe and a NAO$^+$-like circulation anomaly over the North Atlantic.

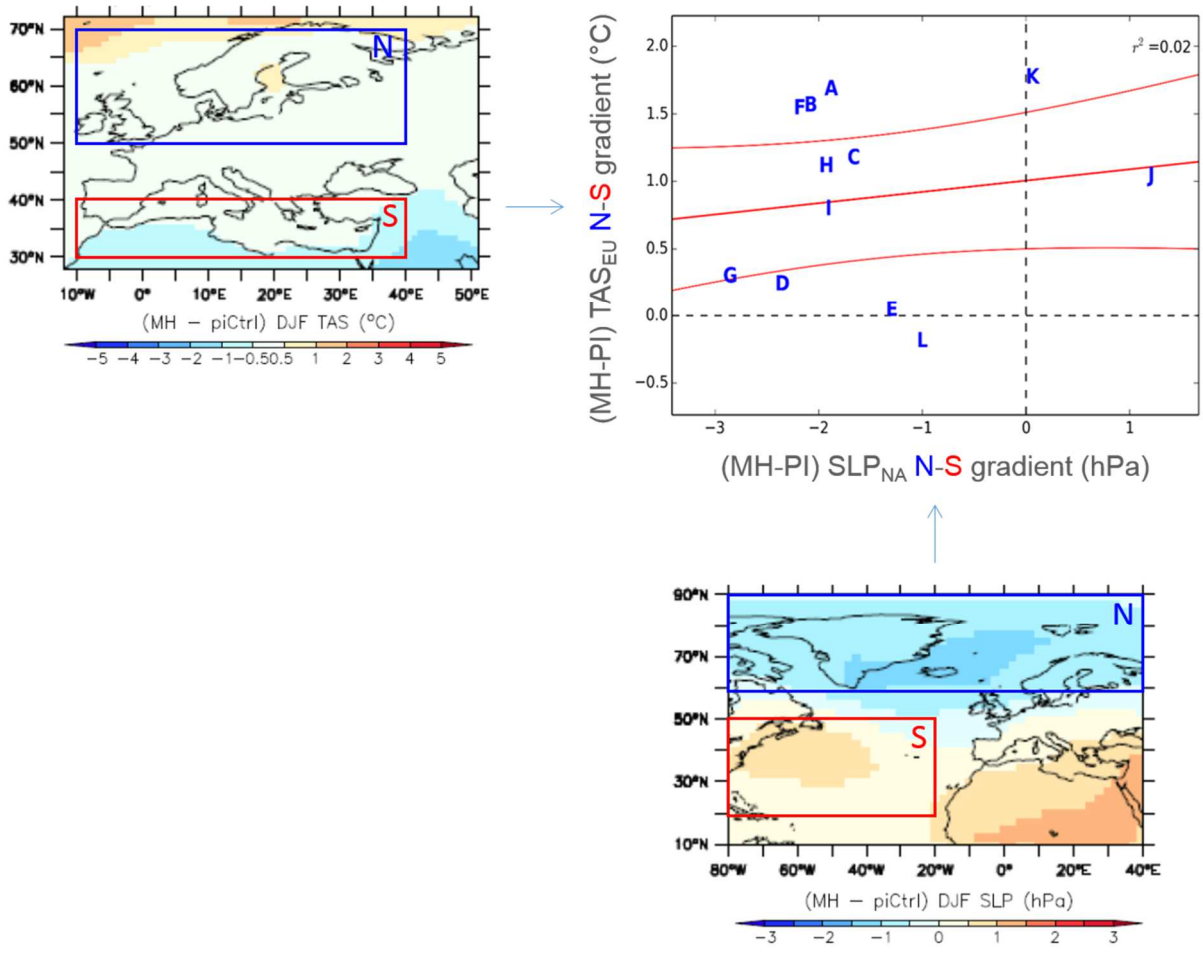

Figure 7: Top left: PMIP3 ensemble mean anomalies of SAT (in °C) in DJF for MH minus PI. The blue box defines the northern region and the red box, the southern region used for calculating the north-shout SAT gradient. Bottom right: PMIP3 ensemble mean anomalies of SLP (in hPa) in DJF for MH minus PI. The blue box defines the northern region and the red box, the southern region used to define the SLP north-south gradient. Top right: Multi-model relationship of the land temperature anomaly gradient (defined in top left panel) - on the y-axis - and the SLP anomaly gradient (defined in bottom right panel) - on the x-axis. The squared correlation coefficient is shown in the top-left corner of the figure. The red lines indicate the linear regression and the 95% confidence interval for this regression.

Factors determining the simulated $\Delta SAT_{DJF,EU}$ meridional gradients

Figure 2 shows that the strongest $\Delta SAT_{DJF, EU}$ signals are found, for most models, close to the latitude boundaries of the region considered. Enlarging the domain of our analysis places the European temperature anomalies patterns in the larger-scale context (Figure 8a). We find that the modeled north-south $\Delta SAT_{DJF, EU}$ contrasts are dominated, to the north, by warm temperature anomalies over the Nordic Seas and, to the south, by cold temperature anomalies over northern Africa. This pattern resembles the reconstruction of the North-South contrast, but there are a number of regional differences. Most notably, the cooling pattern over Ireland is not captured by the climate models, while the warming from the ocean does not penetrate enough inland over Europe.

To a large extent, the negative SAT anomalies over northern Africa (and the positive SLP anomalies) are related to the negative radiative forcing in winter at these latitudes (Figure 1). This anomaly is strongest at low latitudes and has an amplified effect on SAT over continents vs. oceanic regions, possibly due to the lower heat capacity of land than water and to the differences in lapse rates between land and ocean (*e.g.* Joshi et al 2008).

Inter-model differences of ΔSAT over the southern region in Figure 7a are indeed small (0.3ºC inter-model standard deviation) relative to the ones over the northern region (0.8ºC), consistent with a lower ΔSAT inter-model standard deviations over northern Africa than over

315 the Nordic Seas (Figure 8b). Thus, for the rest of the paper we will focus mainly on what
316 determines the inter-model spread in ΔSAT_{DJF} over the Nordic Seas, that dominates the north-
317 south contrast.

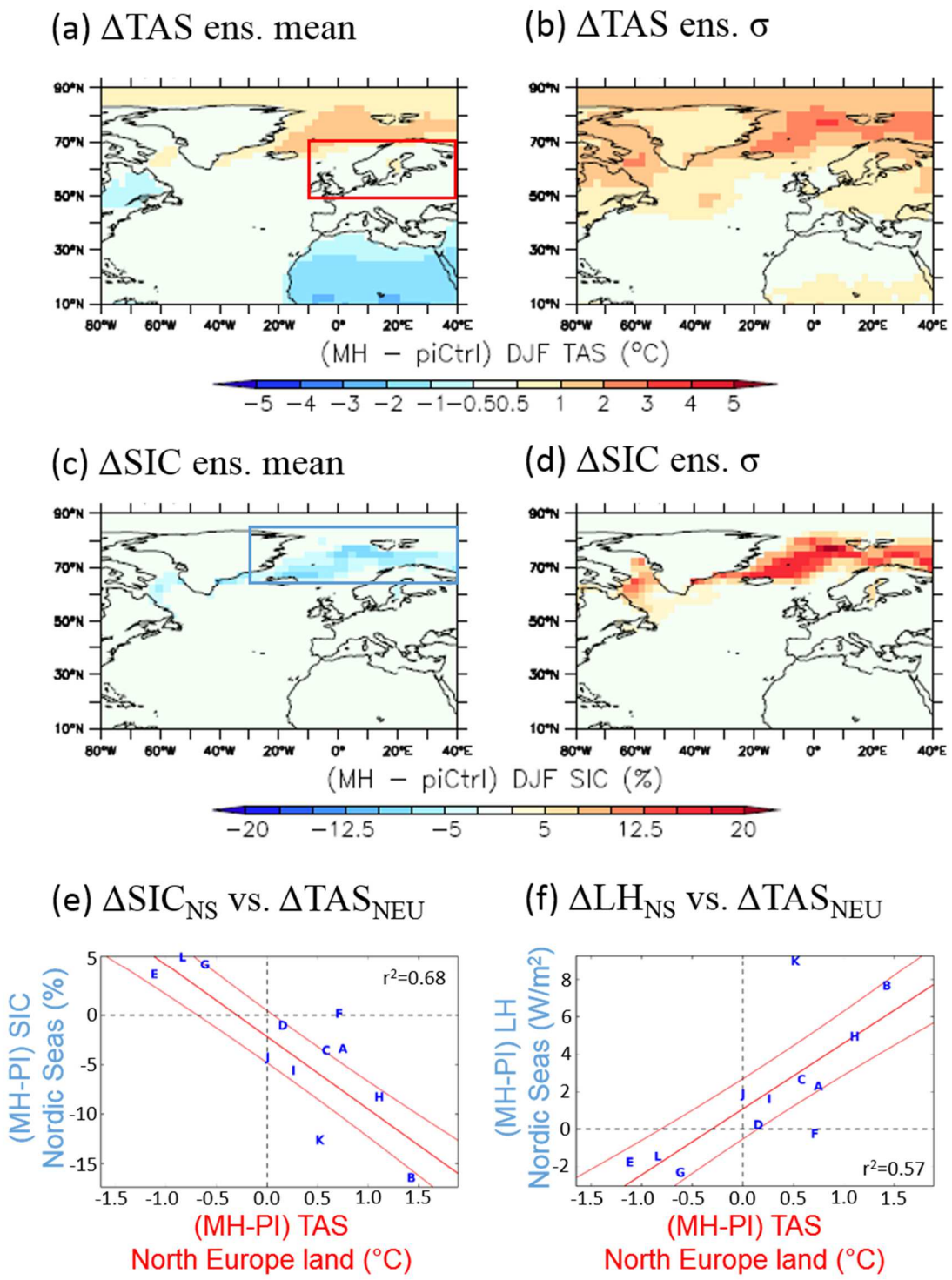

318

319 **Figure 8:** MH winter anomalies of (a, b) near-surface air temperature and (c- d) sea ice cover over the North
320 Atlantic sector. (a) and (c) show the multi-model ensemble mean anomalies and (b) and (d) show the ensemble

standard deviation. (e) Relationship between simulated near-surface air temperature over land in northern Europe and sea ice cover anomalies averaged over the region highlighted in (a) and (c) for the 12 models analyzed. (f) Same as (e) but with sea ice cover anomalies replaced by latent heat flux anomalies from the ocean to the atmosphere. The squared correlation coefficient is show in the top- and, respectively, bottom-left corner of the plots. In both plots, the red lines indicate the linear regression and the 95% confidence interval for the regression.

The spatial patterns of both the ΔSAT_{DJF} signal in the Nordic Seas and its inter-model spread (Figure 8a, b) are strongly reminiscent of those of the DJF sea-ice cover anomalies (Figure 8c, d). Sea-ice cover changes have a strong impact on near-surface temperatures *via* air-sea fluxes and albedo feedbacks (Swingedouw et al. 2006, Årthun et al. 2017). This influence extends to neighbouring land regions: the inter-model differences in ΔSAT_{DJF} in land areas of northern Europe (Figure 8e) are well correlated (r^2=0.68, $p<0.01$) with the differences in ΔSIC_{DJF} over the Nordic Seas. Furthermore, these differences in ΔSAT_{DJF} are also well correlated with the changes in latent heat flux from the ocean to the atmosphere over the Nordic Seas. Thus, we argue that it is the difference in latent heat flux released in winter by the ocean to the atmosphere and associated with the insulation effect of the presence (or not) of sea ice that explains the response of ΔSAT_{DJF} over northern Europe land. A similar mechanism was indeed highlighted by Årthun et al. (2017) to explain the impact of Nordic Seas SST variability on the temperature of Scandinavia.

Thus, to understand the differences between the wintertime MH European temperature anomalies between the models, we mainly need to understand the origins of the differences between the simulated sea ice cover anomalies in the Nordic Seas region.

Origins of winter sea-ice decline

Atmospheric circulation anomalies

While NAO-like anomalies do not directly determine the inter-model differences in winter temperature anomalies over Europe in PMIP3 ensemble, atmospheric circulation changes

between MH and PI winters could potentially control the sea ice anomalies in the Nordic Seas, through anomalous atmospheric heat transport.

To test this hypothesis, we tried to calculate the total atmospheric heat transport into the Nordic Seas region. This computation should be based on changes of both the mean and transient circulation. Unfortunately, the PMIP3 database does not routinely include data at sufficiently high frequencies to allow for the calculation of the latter term, nor does it provide estimates of atmospheric heat transport computed at the model time step. We can thus only offer a partial answer, related to the mean wind anomalies only.

Whether we consider the near-surface horizontal temperature advection due solely to the change in the mean winter near-surface horizontal wind velocities between PI and MH (estimated as $-\Delta\vec{U}\cdot\nabla T_{PI}$, where Δ stands for MH-PI differences, $\vec{U}$ for the horizontal wind velocity and T_{PI} for the temperature for pre-industrial simulation; Figure 9) or the change between the mean circulation-induced horizontal temperature advection in PI vs. MH winters (estimated as $-\Delta(\vec{U}\cdot\nabla T)$; not shown), we find no correlation of these respective anomalies with the winter sea ice cover anomaly over the Nordic Seas region (Figure 9). More generally, two other elements of the energy budget argue against an increased poleward atmospheric transport in MH winter: at the top of the atmosphere, the latitudinal gradient of insolation decreases (with more cooling at lower latitudes), and the ocean heat transport tends to increase (due to AMOC strengthening as shown below). Both would typically lead to a compensating equatorward energy transport by the atmosphere, away from the sea ice region. Such a response has actually been demonstrated in MH simulations run with the IPSL-CM5A-LR model (Saint-Lu et al. 2016). We thus find no evidence that the changes in the atmospheric heat transport may be responsible for ΔSIC_{DJF} in the models.

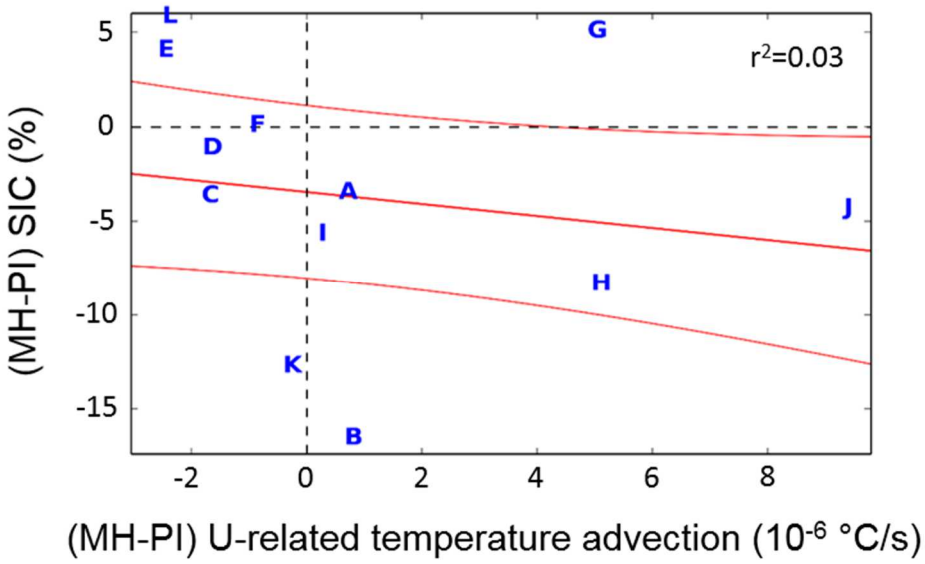

Figure 9: Multi-model relationship between wintertime sea ice cover anomalies and mean 1000hPa horizontal circulation anomaly-related temperature advection in the NS region. The red lines indicate the linear regression and the 95% confidence interval for this regression.

Summer sea ice anomalies

Another potential source of the inter-model differences in winter sea ice anomalies is the summer (JJA) sea ice response, with a memory effect between the two seasons. Indeed, the insolation is far larger in the Mid-Holocene compared to the pre-industrial period during summer (Figure 1), potentially leading to large melting of sea ice and heat storage in the ocean in summer, which may then persist into winter due to the large inertia of the ocean. There is a fine interplay between winter and summer sea ice: winter sea ice thickness heavily influences the ice pack vulnerability to summer melt, and thus has an important effect on summer sea ice cover (Berger et al. 2013). Conversely, summer melt allows for ocean surface heat uptake and renders new sea ice formation more difficult during autumn and winter. Thus, we can also expect a ΔSIC_{JJA} effect on ΔSIC_{DJF} (Berger et al. 2013). This latter effect may play an important role in determining the inter-model ΔSIC_{DJF} differences. Indeed, the different models may exhibit different sea ice responses to the summer radiative forcing (Figure 1) for example through different strength of feedbacks, like the local cloud response

(*cf.* Knudsen et al. 2015; Abe et al. 2015). These differences in summer may then project on the winter responses.

We thus check if the relationship between ΔSIC_{JJA} and ΔSIC_{DJF} is consistent between the models. Figure 10 indeed shows a strong multi-model relationship between ΔSIC_{JJA} and ΔSIC_{DJF}, both globally over the Northern Hemisphere high latitudes (r^2=0.74, p<0.01), and regionally over the Nordic Seas (r^2=0.73, p<0.01).

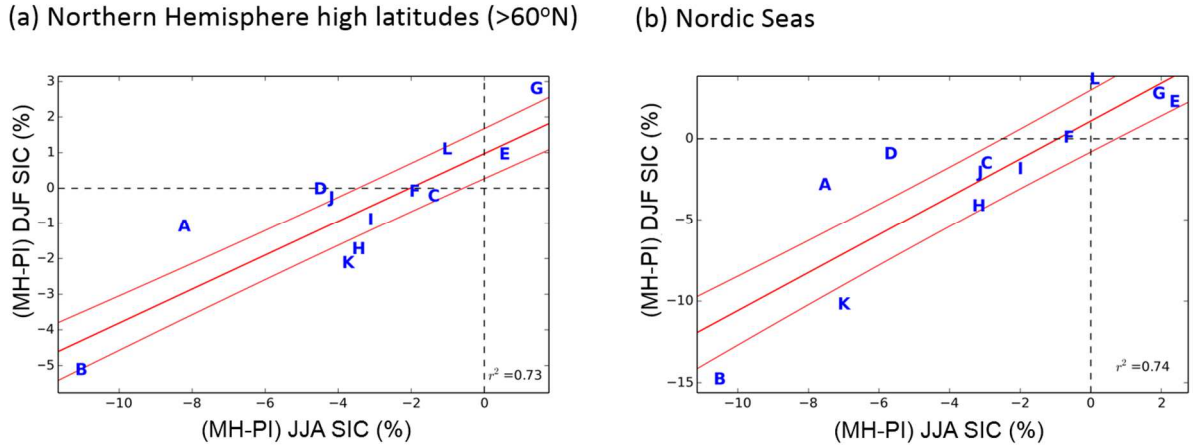

Figure 10: Relationship between MH winter and summer sea ice cover anomalies (a) averaged over the Northern Hemisphere high latitudes (above 60°N); (b) averaged over the Nordic Seas (rectangular region contoured in Figure 8a, c). The text boxes in the bottom-left corner of the figures show the associated squared correlation coefficients. The red lines indicate the linear regressions and the 95% confidence interval for the regressions.

While it is likely that a memory of the seasonally forced ΔSIC_{JJA} can influence ΔSIC_{DJF}, it is also possible that both summer and winter sea ice anomalies are influenced by a large-scale, common factor such as a change in the Atlantic meridional overturning circulation (AMOC), which we investigate in the following section.

Change in the AMOC

Figure 11 shows the changes in the AMOC between the simulated MH and PI climates. All 12 models analyzed show significant anomalies in the mean AMOC, with considerable inter-

model variability in terms of both anomalies (Figure 11, colors) and background state (PI AMOC – Figure 11, contours). In general, the AMOC is strengthened in MH compared to PI. This is consistent with Born et al. (2010), who proposed that for a climate with warmer summer (the Eemian in their case), the decrease in sea ice transport through Fram Strait may change the salinity in the Labrador Sea and enhance local convective activity, feeding a stronger AMOC.

AMOC MH anomalies vary between models not just in terms of intensity, but also in terms of structure, complicating their quantitative comparison. Nevertheless, maxima of the meridional stream function have been shown to be strongly related to the meridional ocean heat transport (*e.g.* Boning et al. 1995). Thus, they represent a reasonable parameter to consider in the investigation of sea ice changes.

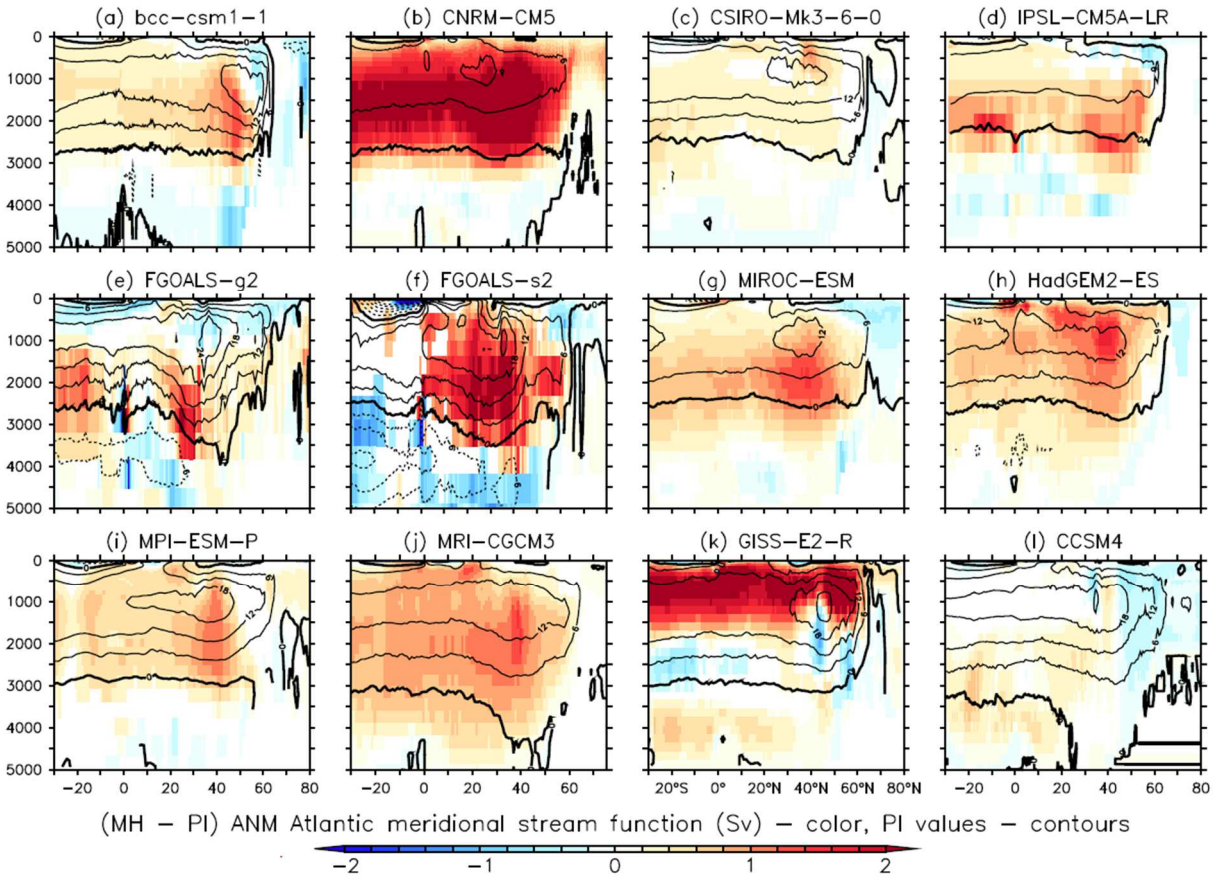

418 **Figure 11**: Color: significant (at 90% level) MH anomalies of the climatological annual mean (ANM) Atlantic
419 meridional stream function; contours: PI climatologies (contour spacing: 6 Sv; solid/dashed contours represent
420 positive/negative values) for the 12 models analyzed.

421 Figure 12 shows the relationship between winter sea-ice cover anomalies and anomalies in the
422 maximum of the climatological Atlantic meridional stream function at three different
423 latitudes: 26^{o}N and 45^{o}N, typically used when describing the AMOC strength (*e.g.*, Huck et
424 al. 2008, McCarthy et al. 2015), and 60^{o}N, closer to the Nordic Seas region. The DJF SIC
425 anomalies are in all cases negatively correlated with the AMOC strength anomalies. The
426 correlation coefficient and the slope of the corresponding linear regressions increase with
427 latitude, so that the strongest link of $\Delta SIC_{DJF,NS}$ with the meridional ocean circulation is found
428 for ΔAMOC at 60^{o}N. The correlation coefficient is 0.89 (p-value < 0.01) and the linear
429 regression line has a near-zero intercept, indicating that, as would be expected, an
430 intensification of the AMOC at high latitudes is linearly associated to negative SIC anomalies
431 in the Nordic Seas and *vice-versa*. The correlation remains high even at 26°N (r=0.75,
432 p<0.01), indicating that this relationship is not a purely local effect. Nevertheless, the
433 relationships we find are very sensitive to the low number of models, and removing a few of
434 them can strongly lower the correlation.

435 Changes in the subpolar gyre may also strongly affect the heat transport to the high latitudes
436 (Born et al. 2015). However, the barotropic stream function was not available for all the
437 models, limiting the analysis of this effect. Since the strength of the subpolar gyre is closely
438 related to the strength of the convection in the subpolar gyre (Born et al. 2015), we suggest
439 that the changes in AMOC would also be reflected in subpolar gyre strength, both leading to
440 an increase of meridional heat transport.

441 The changes in oceanic heat transport act on longer than seasonal time scales and may thus
442 affect sea ice cover in both winter and summer, likely contributing to the correlation between

443 winter and summer anomalies highlighted in former sub-section. Nevertheless, direct changes
444 in summer sea ice in response to changes in insolation are also due to regional sensitivity and
445 feedbacks that may differ among the models (*e.g.*, Massonnet et al. 2012), and so could
446 remain a relatively independent factor from AMOC strengthening to explain the inter-model
447 spread.

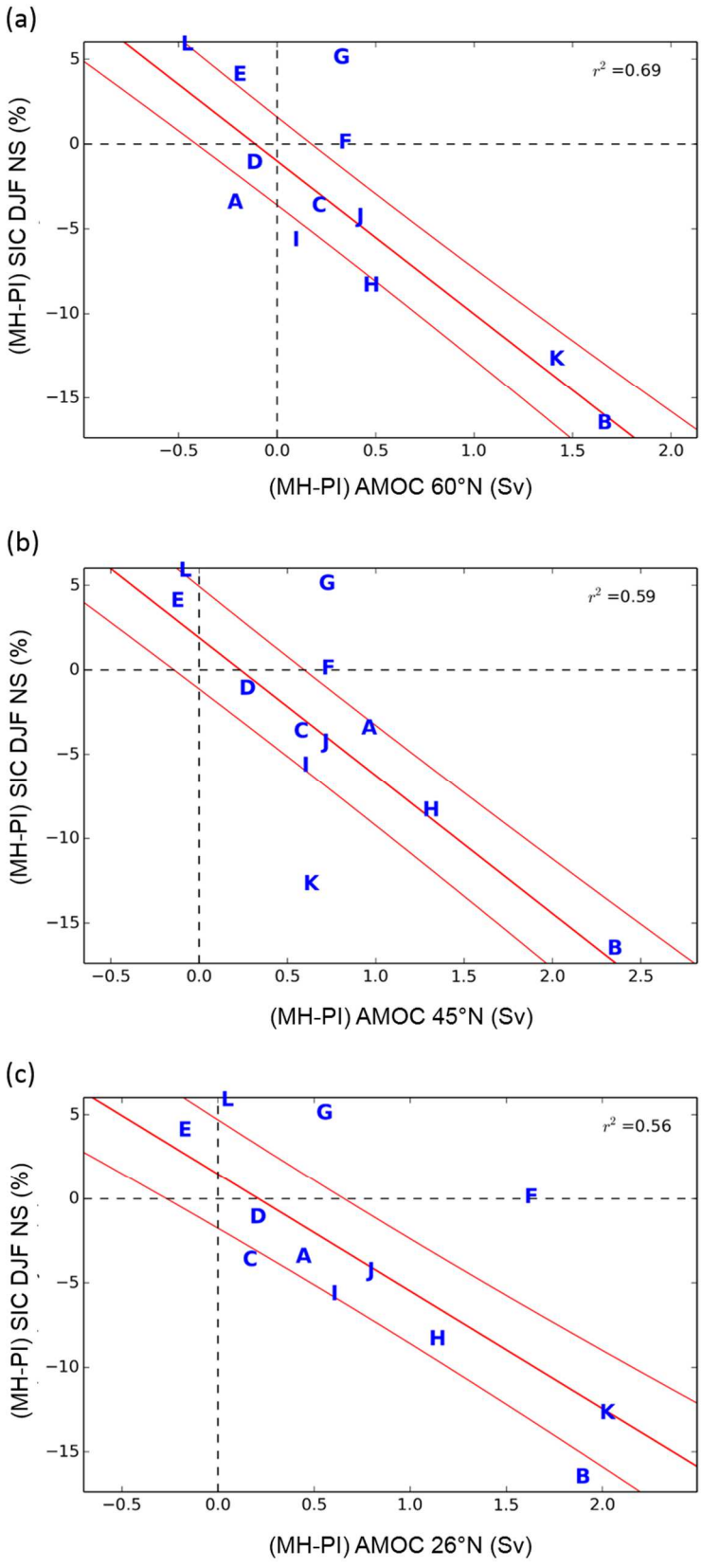

448

449 **Figure 12:** Relationship between mean winter MH sea ice cover anomalies over the Nordic Seas region and the
450 MH anomaly in the maximum climatological Atlantic meridional stream function at (a) 60ºN, (b) 45ºN and (c)
451 26ºN. The squared correlation coefficients of the associated linear regressions are shown in the respective panels.

The correlations are significant above the 99% level. The red lines indicate the linear regression and the 95% confidence interval for this regression.

Combination of multiple factors

In the previous subsections we analyzed one-to-one relationships between $\Delta SIC_{DJF,NS}$ and a suite of atmospheric and oceanic variables. However, the inter-model differences in the winter sea ice anomalies are most likely explained by a combination of different factors which affect the sea ice cover in different measures depending on the model.

We have investigated a wide array of variable combinations to best explain the inter-model variations in $\Delta SIC_{DJF,NS}$ through multiple linear regressions. We have considered parameters physically linked with the winter sea ice anomalies, like the temperature advection due to the mean circulation change in the Nordic Seas region, the surface downward radiative flux anomalies, the background state (PI) sea ice cover, the summer sea ice cover anomalies and the change in the AMOC strength.

The low number of climate simulations (12), the reductive framework (lack of sensitivity experiments) and the intrinsic high level of connectivity between climate variables through non-linear relationships (*i.e.*, variables not independent) limit the potential of such a multivariate analysis. Nevertheless, some information can be distilled on the basis of this exercise.

While in most combinations and for most predictor variables, the high p-values associated to their respective coefficients did not allow for significant regressions, the p-values associated to the coefficient for the AMOC strength anomaly at 60°N were always very small (on the order of 10^{-4}-10^{-5}) and the coefficients themselves were always found to be negative, indicating a robust effect of ΔAMOC on $\Delta SIC_{DJF,NS}$ in the direction already described in the former section.

One multiple linear regression did yield significant results:

$$\Delta SIC_{DJF,NS} = \alpha_0 + \alpha_1 \Delta AMOC_{max.60^oN} + \alpha_2 \Delta SIC_{JJA,NS} \quad (1)$$

with $p_{\alpha_0} = 0.04$, $p_{\alpha_1} = 10^{-4}$, $p_{\alpha_2} = 4 \cdot 10^{-5}$ and an adjusted r^2 of 0.96.

Figure 13 shows the results of the multiple linear regression model in Eq. 1. Figure 13a shows the good correspondence between the reconstructed and original $\Delta SIC_{DJF,NS}$ and Figure 13b shows, for each model, the percentage of the sea ice cover change associated with each term in the regression model. According to the model of Eq. (1), the summer sea ice anomalies and AMOC strength anomalies have comparable effects on $\Delta SIC_{DJF,NS}$, with the AMOC playing a particularly important role in FGOALS-s2 and CCSM4, as well as in GISS-E2-R, HadGEM2-ES, MRI-CGCM3, CNRM-CM5 and MPI-ESM-P where the AMOC term represents more than 50% of the total change.

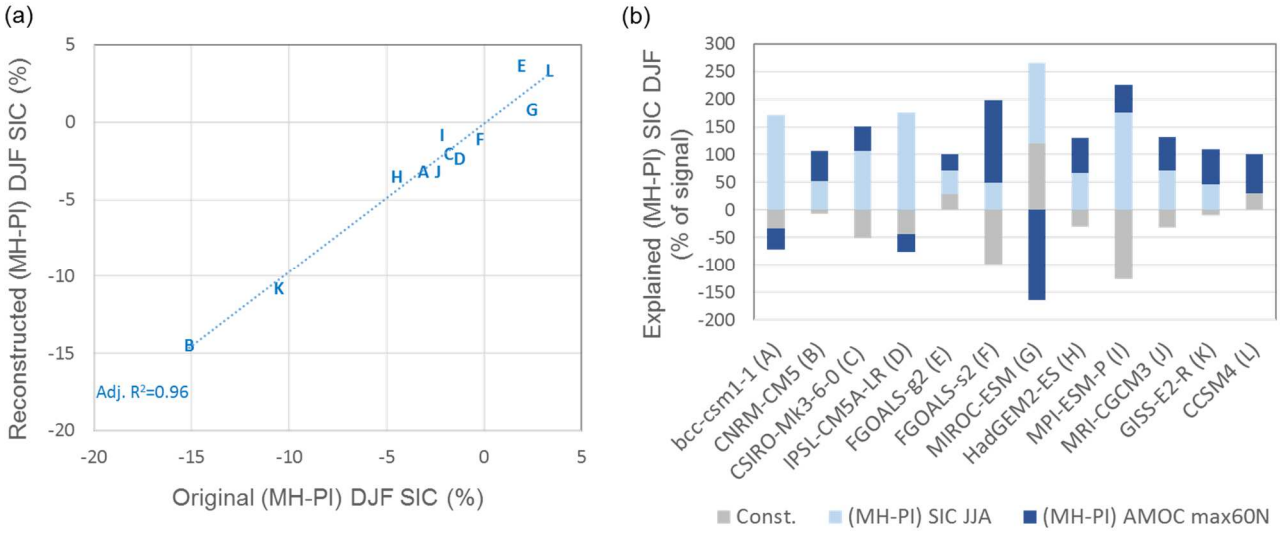

Figure 13. Results of the multiple linear regression of $\Delta SIC_{DJF,NS}$ onto the MH anomaly of the AMOC maximum at 60ºN and $\Delta SIC_{JJA,NS}$: (a) correspondence of the reconstructed and original $\Delta SIC_{DJF,NS}$; (b) fraction of the simulated winter sea ice cover anomaly associated to each model predictor, for the 12 models analyzed.

The adjusted r^2 can be mildly improved (to a value of 0.97) by adding the pre-industrial sea ice cover over the Nordic Seas region, $SIC_{DJF,PI,\ NS}$, as an extra predictor. However, the associated p-value is 0.015, indicating a 1.5% chance that this predictor has in fact no effect on $\Delta SIC_{DJF,NS}$. Furthermore, the coefficient for this extra term is positive in this regression model (indicating that climate models where more winter sea ice is present in the Nordic Seas region in pre-industrial simulations tend to have positive or less negative Mid-Holocene winter sea ice anomalies) but is negative in all other variable combinations analyzed. The role, if any, of the background sea ice cover on the $SIC_{DJF,\ NS}$ anomalies thus remains uncertain.

The main caveat of the model in Eq (1) is that the two predictor variables are not independent. $\Delta AMOC_{max,60°N}$ and $\Delta SIC_{JJA,NS}$ are correlated with an r^2 of 0.34, significant at the 95% level. It is indeed very likely that the AMOC anomaly affects winter sea ice both directly, through oceanic heat transport in winter, and indirectly, by influencing sea ice anomalies during summer which, in turn, through ocean-sea ice-atmosphere feedbacks, can have a lasting effect on the winter anomalies. Nevertheless, the AMOC may be affecting the annual sea ice anomalies and, since sea ice seasonality is model-dependent, adding the summer sea ice as a second predictor improves the results of the regression analysis. Such a regression could thus allow to explain some of the spread that can be explained by local sea ice feedback and not only the AMOC changes.

Summer sea ice cover anomalies are actually not entirely determined by the AMOC differences. As shown in Figure 1, the Mid-Holocene experiences an important positive summer radiative forcing in the high latitudes and the sensitivity of each model to this forcing is very likely to have a strong effect on the summer sea ice anomalies. Since Mid-Holocene forcing is seasonal and unevenly distributed over the globe, classical definitions of climate sensitivity do not apply and could not be used to directly evaluate the model sensitivity effect

516 on $\Delta SIC_{JJA,NS}$ and thus on $\Delta SIC_{DJF,NS}$. We have attempted to use different first-order proxies
517 of this effect that would be less correlated with the AMOC change (such as summer SAT or
518 surface downward shortwave radiation anomalies over large domains in the Northern
519 Hemisphere) as a replacement for $\Delta SIC_{JJA,NS}$ in the regression model above, but with
520 unsatisfactory results in terms of p-values and correlation coefficients.

521 **Link with future projections**

522 In order to estimate if simulated changes in the AMOC for the mid-Holocene are connected
523 with its behavior in climate projections, we have processed data from RCP85 projections. We
524 found 10 models from our PMIP3 pool that provide data for these projections. The scatterplot
525 of the anomalies in projections *vs.* anomalies for mid-Holocene is shown in Figure 14. A
526 significant correlation at the 95% level is found between the two, showing that models
527 simulating a stronger AMOC in the mid-Holocene also tend to simulate a stronger weakening
528 of the AMOC in RCP85 projections. This may indicate that models with a high AMOC
529 sensitivity to changes in mid-Holocene conditions also show a higher sensitivity of the
530 AMOC in future projections. Thus, constraining the changes in the AMOC for the mid-
531 Holocene may constitute a potential emergent constraint to reduce the very large uncertainty
532 of the AMOC response in future climates. Nevertheless, the relatively low correlation found
533 limits this interpretation. Also, quantitative estimates of AMOC variations over the Holoecne
534 are lacking, even though a few qualitative reconstructions exist (Kissel et al. 2013, Ayache et
535 al. 2018) and indicate that the AMOC may have been relatively intense during the mid-
536 Holocene.

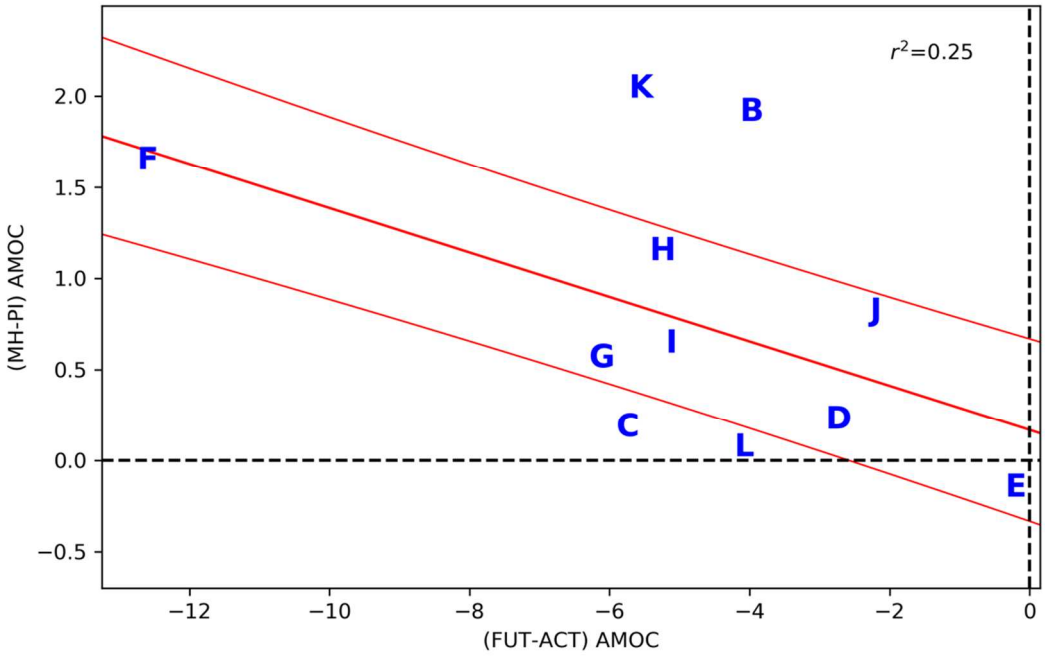

Figure 14. Relationship between mean AMOC anomalies in mid-Holocene relative to preindustrial simulations and projections following an RCP85 scenario for the period 2081-2100 as compared to present-day period 2006-2015.

Discussion and conclusions

We have analyzed Mid-Holocene winter anomalies over the North Atlantic sector in 12 PMIP3 models with the purpose of comparing the simulated European winter temperature anomalies with reconstructed data, and shedding light on their drivers.

Comparing the simulated winter near-surface air temperature anomalies with the recent pollen-based reconstruction of Mauri et al. (2014) for the Mid-Holocene, we found some qualitative agreement with the paleo-reconstruction for a few models, with pattern correlation coefficients above 0.6 for 5 out of the 12 models, mostly reflecting a north-south temperature anomaly gradient over Europe. All models underestimate the amplitude of the winter anomalies, however, as well as the amplitude of this meridional gradient and the exact anomaly pattern, compared to the Mauri et al. (2014) reconstruction. Nevertheless, the

552 uncertainties of this reconstruction do allow for a weaker gradient as found in some of the
553 models.

554 To understand the simulated response to mid-Holocene (MH) forcing, we have first analyzed
555 the simulated large-scale atmospheric circulation anomalies over the North Atlantic sector.
556 Our analysis has revealed a consistent climatological winter atmospheric response in mid-
557 Holocene consisting of two elements common to all models, though varying in spatial extent
558 and intensity. The first is a dynamically forced anti-cyclonic anomaly over the south-western
559 part of the North Atlantic, with a strong barotropic component. This structure is associated
560 with a local weakening of the jet stream and a more pronounced separation between the eddy-
561 driven and subtropical jet streams over the North Atlantic sector. The second element is a
562 positive sea-level pressure anomaly over northern Africa with a shallow baroclinic structure.
563 This SLP anomaly is a result of the colder atmospheric temperature in response to the strong
564 negative radiative forcing at low latitudes, the effects of which are amplified over continental
565 regions. In the same way, a shallow low-pressure anomaly is found in the north of the basin,
566 in thermal balance with positive temperature anomalies. For some models these SLP
567 anomalies could be interpreted as a NAO^+ signal, although the vertical structure of the NAO
568 is much more barotropic.

569 While some models exhibit a NAO^+-like atmospheric circulation anomaly near the surface in
570 winter, the ensemble of 12 PMIP3 models does not support a link between this type of large-
571 scale atmospheric response and the MH temperature anomaly patterns over Europe. Instead,
572 the simulated MH European winter temperature anomaly patterns are, in most models,
573 determined by the radiatively forced cold anomalies at low latitudes and the more model-
574 dependent sea ice anomalies over the Nordic Seas, with the latter responsible for
575 approximately three times more inter-model variability than the former.

576 The analyses carried out to understand the differences in these sea ice anomalies between the
577 models have revealed multiple footprints of the ΔSIC feedbacks onto other fields often
578 dominating the climatological anomalies in the Nordic Seas region. We have shown here the
579 signature of these feedbacks on the near-surface air temperature, but similar signatures have
580 also been found (not shown) on other variables. A very tight collocation between strong
581 negative (positive) sea ice anomalies and negative (positive) near-surface horizontal wind
582 divergence anomalies was found in all models for which the latter could be calculated, likely
583 explained by a response of the near-surface atmospheric circulation to the sea ice anomalies
584 and to the associated air-sea flux anomalies. A local increase in cloud cover over negative
585 ΔSIC regions (and *vice-versa*) has been found in most models, engendering marked local
586 anomalies of the downward longwave and shortwave radiative fluxes at the surface (positive
587 and negative respectively over regions of sea ice loss and *vice-versa*). A strong ΔSIC
588 feedback has also been found on the surface sensible heat flux (SH). In 3 out 12 models this
589 corresponds to a simple positive response of SH to a positive ΔSIC or *vice-versa*. In most
590 models, however, the response is more complex, taking the form of a strong positive-negative
591 SH dipole over the ΔSIC region depending on the background sea ice cover, which shows a
592 subtle interplay of sea surface temperature and air temperature anomalies in these regions.

593 These ubiquitous sea ice feedback signatures confirm the importance of a correct sea ice
594 representation in the models for representing the regional climate over Europe. All but three
595 models show a reduced winter sea ice cover in the Nordic Seas region in mid-Holocene
596 compared to the pre-industrial climate. While not allowing for a quantitative model evaluation
597 of the sea-ice cover anomaly, a recent compilation of multi-proxy reconstructions of mid-
598 Holocene ΔSIC which expands on the data set used in Klein et al. (2014) (Seidenkrantz, 2015,
599 personal communication) qualitatively confirms this result. Nevertheless, the publication of
600 this compilation will be necessary to establish any strong observational constraints on this
601 aspect. Based on this on-going work of compilation, we can suggest that an increase in Nordic

602 Seas winter sea ice cover in the mid-Holocene, namely in FGOALS-g2, MIROC-ESM and
603 CCSM4, are not in line with the few available data for the MH climate in the North Atlantic
604 sector. It remains unclear if these mismatches are due to a poor response of the sea ice system
605 to insolation or are related to an ocean circulation response and its influence on the sea ice.

606 Sea ice feedback signatures dominating the climatological winter anomalies hinder the quest
607 for the causes of SIC anomalies in the model results. Nevertheless, we were able to highlight
608 a robust multi-model relationship between the MH winter SIC anomalies in the Nordic Seas
609 region and the anomalies in the Atlantic meridional overturning circulation, which points to
610 the AMOC as an important driver of the MH response of European winter temperatures.

611 The MH-PI differences in the atmospheric heat transport due to transient eddies form an
612 important potential source of information on the drivers of the SIC anomalies. However, these
613 differences could not be evaluated due to the lack of availability of the corresponding fields in
614 the PMIP3 data base. This type of drawback will be solved thanks to the inclusion of such
615 fields in the outputs from future model intercomparison exercises such as the upcoming
616 CMIP6 and PMIP4.

617 Another potential key player neglected here is the feedback from vegetation changes in the
618 high latitudes, which could also amplify the pattern found in the MH simulations (Wohlfahrt
619 et al. 2008), potentially bringing the model simulations closer to MH observations.

620 We also know that PMIP3 models systematically underestimate the monsoon anomalies in the
621 mid-Holocene (the “Green Sahara” event, Claussen & Gayler 1997). It is plausible that this
622 event was linked to a northward shift of the Hadley Cell (Claussen and Gayler 1997), which
623 would therefore not be captured, or, at best, be severely underestimated by the models. We
624 conjecture that all models underestimate large-scale anomalies in the atmospheric circulation
625 that may have taken place (Gaetani et al. 2017) and may have affected temperature patterns

626 over Europe during MH winters. Our study, however, highlights the potential relevance of
627 other effects, which deserve further study.

628 While previous, paleo-reconstruction-based studies, often attribute mid-Holocene winter
629 European temperature anomalies to a NAO^{+}-like atmospheric circulation anomaly, our
630 analysis of PMIP3 models suggests the possibility of an additional or even alternative
631 explanation coming from a larger geographical context. In this new view, based on the most
632 skillful PMIP3 models, European winter temperature anomaly patterns are determined, to the
633 south, by strong low-latitude temperature responses to the seasonal negative radiative forcing
634 and to the north by feedbacks of the negative sea ice anomalies over the Nordic Seas on the
635 atmosphere. Model simulations also suggest that a major driving force for these sea ice
636 anomalies is an intensification of the Atlantic meridional overturning circulation in the mid-
637 Holocene compared to the modern period, as indirectly suspected in Masson et al. (1999).
638 This is in agreement with reconstructions based on sortable silt in the North Atlantic, a proxy
639 of deep water circulation, which indicate a stronger deep current during the MH (Kissel et al.
640 2013). The amplitude of the north-south gradient over Europe is weaker in the models than in
641 the reconstruction. We can suggest that this is related to a general bias of climate models in
642 representing the strong air-sea interaction as recently highlighted by the so-called signal to
643 noise paradox by Scaife et al. (2018).

644 The summertime temperature reconstruction from Mauri et al. (2014) does not show any
645 agreement with model simulations and leads to very different patterns than the model
646 simulations (not shown, *cf.* Mauri et al. 2014). This weakens the hypothesis expressed here.
647 The analysis of the differences between models and reconstruction data is out of the scope of
648 the present paper and deserves a dedicated study. Nevertheless, we can highlight here that
649 changes in the AMOC mainly affect European temperature in winter (*e.g.* Figure 4 from

650 Jackson et al. 2015), and may have a far weaker signature on summer temperatures, where
651 other processes might be dominant.

652 The cause for the differences in the AMOC has not been analyzed in the present paper, as it
653 will also necessitate a dedicated study. As noticed before, this could be related to a decrease
654 in sea ice transport through the Fram Strait due to a lower sea ice production when insolation
655 is larger in summer (Born et al. 2010). This shows that the AMOC is not only influencing the
656 sea ice, but could also be modified by it, implying a two-way feedback also potentially at play
657 in the Nordic Seas. Another interesting factor could be related to the influence of the
658 atmospheric circulation on the AMOC. For instance, variability of the AMOC over the last 60
659 years has often been related to NAO variations (Delworth et al. 2016; Swingedouw et al.
660 2015b). The mechanism is related to a cooling of the surface Labrador Sea during NAO^+
661 phases, which increases the Labrador deep water formation and, a few years later, the AMOC
662 (Eden and Willebrand 2001). Thus, if the atmospheric circulation during the MH changed
663 towards a NAO^+-like configuration, then it likely amplified the AMOC, as highlighted in Shi
664 and Lohman (2016) for the ECHAM-FESOM-MPIOM climate model. In the MH PMIP3
665 ensemble, however, the NAO changes are not the main driver, since our indices of NAO and
666 AMOC changes are not significantly correlated (not shown).

667 If this interpretation is correct, then the MH European winter temperatures may be a test-bed
668 to estimate possible changes in sea ice and in the AMOC in the near future, with the role of
669 the NAO to be further investigated in larger multi-model ensembles. Since, as we find here,
670 the inter-model differences in MH temperature anomalies are mainly explained by AMOC
671 changes, we conclude that the MH is indeed an interesting case study to evaluate the
672 sensitivity of the simulated AMOC to changes in radiative forcing. Indeed, changes in the
673 simulated AMOC for RCP85 projections generally exhibit strong weakening in models that
674 show large strengthening for mid-Holocene. The linear relationship is nonetheless not very

strong and the interpretation is limited by the low number of models analyzed here. The proof of concept presented here will thus benefit from a higher number of models, which will be hopefully reached within CMIP6.

Furthermore, to produce a correct assessment of models, we need to have a finer, quantitative AMOC reconstruction for this period. The use of a methodology combining climate models and available observational datasets, as employed for the deglaciation by Ritz et al. (2013) for instance, is an interesting approach to be developed. This may help to better decipher the sensitivity of the AMOC to different forcings, which could then provide new leads to reduce the very large uncertainty (Weaver et al. 2012) concerning the future of the AMOC. For this purpose, the use of more models available with paleo-configuration will be a key prerequisite, since the analysis led here clearly suffers from the low number of models available within CMIP5.

Acknowledgements

We wish to thank Marrit-Solveig Seidenkrantz, Hugues Goosse and Frédéric Hourdin for fruitful discussions that have benefitted our study. This project would not have been possible without the availability of PMIP3 data in a centralized, consistent format, for which we are deeply thankful to the climate modeling centers listed in Table 1, to the groups behind the ESGF portal, and in particular to Guillaume Levavasseur and Jean-Yves Peterschmitt, as well as the FileFinderAR5 developed by Patrick Brockmann. To analyze the PMIP3 data, this study benefited from the IPSL Prodiguer-Ciclad facility supported by CNRS, UPMC, Labex L-IPSL which is funded by the ANR (Grant #ANR-10-LABX-0018) and by the European FP7 IS-ENES2 project (Grant #312979). AGB was supported by the Swedish Research Council Grant No. C0629701 (MILEX). The research leading to this study also received funding from the French National Research Agency HAMOC project (Grant ANR-13-BS06-0003). This research was supported by the Blue-Action project (European Union's Horizon

2020 research and innovation programme, grant number: 727852) and the EUCP project (European Union's Horizon 2020 research and innovation programme under grant agreement no 776613).

References

Årthun, M. et al. (2017) Skillful prediction of northern climate provided by the ocean. Nat. Commun. 8, 15875 doi: 10.1038/ncomms15875.

Ayache M. Swingedouw D., Mary Y., Eynaud F., Colin C. (2018) AMOC variability over the Holocene: A new reconstruction based on multiple proxy-based SST records. *Global and Planetary Changes* 170, pp. 172-189.

Bakker, P., and Coauthors, 2016: Fate of the Atlantic Meridional Overturning Circulation – Strong decline under continued warming and Greenland melting. *Geophys. Res. Lett.*, 1–9, doi:10.1002/2016GL070457. http://onlinelibrary.wiley.com/doi/10.1002/2016GL070457/abstract.

Bao, Q., and Coauthors, 2013: The Flexible Global Ocean-Atmosphere-Land system model, Spectral Version 2: FGOALS-s2. *Adv. Atmos. Sci.*, **30**, 561–576, doi:10.1007/s00376-012-2113-9.

Berger, M., J. Brandefelt, and J. Nilsson, 2013: The sensitivity of the Arctic sea ice to orbitally induced insolation changes: A study of the mid-holocene paleoclimate modeling intercomparison project 2 and 3 simulations. *Clim. Past*, **9**, 969–982, doi:10.5194/cp-9-969-2013.

Boning, C. W., F. O. Bryan, W. R. Holland, and R. Doscher, 1995: Deep water formation and meridional overturning in a high-resolution model ofthe North Atlantic. *J. Phys. Oceanogr.*, **26**, 1142–1164.

Born, A., K. H. Nisancioglu, and P. Braconnot, 2010: Sea ice induced changes in ocean

circulation during the Eemian. *Clim. Dyn.*, **35**, 1361–1371, doi:10.1007/s00382-009-0709-2.

Born, J. Mignot and T.F. Stocker (2015) Multiple Equilibria as a Possible Mechanism for Decadal Variability in the North Atlantic Ocean. *Journal of Climate* **28**, 8907-8922

Braconnot, P., S. P. Harrison, M. Kageyama, P. J. Bartlein, V. Masson-Delmotte, A. Abe-Ouchi, B. Otto-Bliesner, and Y. Zhao, 2012: Evaluation of climate models using palaeoclimatic data. *Nat. Clim. Chang.*, **2**, 417–424, doi:10.1038/nclimate1456. http://dx.doi.org/10.1038/nclimate1456.

Brewer, S., Guiot, J., and Torre, F.: Mid-Holocene climate change in Europe: a data-model comparison, Clim. Past, 3, 499-512, https://doi.org/10.5194/cp-3-499-2007, 2007.

Cattiaux, J., and C. Cassou, 2013: Opposite CMIP3/CMIP5 trends in the wintertime Northern Annular Mode explained by combined local sea ice and remote tropical influences. *Geophys. Res. Lett.*, **40**, 3682–3687, doi:10.1002/grl.50643.

Chabaud, L., M. F. Sanchez Goni, S. Desprat, and L. Rossignol, 2014: Land-sea climatic variability in the eastern North Atlantic subtropical region over the last 14,200 years: Atmospheric and oceanic processes at different timescales. *The Holocene*, **24**, 787–797, doi:10.1177/0959683614530439.

Claussen, M., and V. Gayler, 1997: The Greening of the Sahara during the Mid-Holocene: Results of an Interactive Atmosphere-Biome Model. *Glob. Ecol. Biogeogr. Lett.*, **6**, 369–377.

Collins, W. J., N. Bellouin, N. Gedney, P. Halloran, T. Hinton, J. Hughes, and C. D. Jones, 2011: Model Development Development and evaluation of an Earth-System model – HadGEM2. 1051–1075, doi:10.5194/gmd-4-1051-2011.

Conil, S., and L. Z.-X. Li, 2005: Linearity of the Atmospheric Response to \textsc{N}orth

748 \textsc{A}tlantic SST and Sea Ice Anomalies. *J.\ Clim.*, **18**, 1986–2003.
749 http://dx.doi.org/10.1175/JCLI3388.1.

750 Davis, B. A. S., and S. Brewer, 2009: Orbital forcing and role of the latitudinal
751 insolation/temperature gradient. *Clim. Dyn.*, **32**, 143–165, doi:10.1007/s00382-008-
752 0480-9.

753 Delworth, T. L., F. Zeng, G. A. Vecchi, X. Yang, L. Zhang, and R. Zhang, 2016: The North
754 Atlantic Oscillation as a driver of rapid climate change in the Northern Hemisphere. *Nat.*
755 *Geosci.*, **9**, 509–512, doi:10.1038/ngeo2738.

756 Deser, C., R. Knutti, S. Solomon, and A. S. Phillips, 2012: Communication of the role of
757 natural variability in future North American climate. *Nat. Clim. Chang.*, **2**, 775–779,
758 doi:10.1038/nclimate1562. http://dx.doi.org/10.1038/nclimate1562.

759 Dufresne, J. L., and Coauthors, 2013: *Climate change projections using the IPSL-CM5 Earth*
760 *System Model: From CMIP3 to CMIP5*. 2123-2165 pp.

761 Eden, C., and J. Willebrand, 2001: Mechanisms of interannual to decadal variability of the
762 North Atlantic circulation. *J. Clim.*, **14**, 2266–2280, doi:10.1175/1520-
763 0442(2001)014<2266:MOITDV>2.0.CO;2.

764 Escudier, R., J. Mignot, and D. Swingedouw, 2013: A 20-year coupled ocean-sea ice-
765 atmosphere variability mode in the North Atlantic in an AOGCM. *Clim. Dyn.*, **40**, 619–
766 636.

767 Fischer, N., and J. H. Jungclaus, 2011: Evolution of the seasonal temperature cycle in a
768 transient Holocene simulation: Orbital forcing and sea-ice. *Clim. Past*, **7**, 1139–1148,
769 doi:10.5194/cp-7-1139-2011.

770 Fischer et al. (2018) Palaeoclimate constraints on the impact of 2 °C anthropogenic warming
771 and beyond. Nat. Geosc. 1, 474-485.

772 Gaetani M., Messori G., Zhang Q., Flamant C., Pausata F. S. R. (2017) Understanding the
773 mechanisms behind the northward extension of the West African Monsoon during the
774 Mid-Holocene. *Journal of Climate*, American Meteorological Society, 2017, 30 (19),
775 pp.7621-7642.

776 Gent, P. R., and Coauthors, 2011: The community climate system model version 4. *J. Clim.*,
777 **24**, 4973–4991, doi:10.1175/2011JCLI4083.1.

778 Gladstone, R. M., and Coauthors, 2005: Mid-Holocene NAO: A PMIP2 model
779 intercomparison. *Geophys. Res. Lett.*, **32**, 1–4, doi:10.1029/2005GL023596.

780 Goosse, H., F. Selten, R. Haarsma, and J. Opsteegh, 2002: A mechanism of decadal
781 variability of the sea-ice volume in the Northern Hemisphere. *Clim. Dyn.*, **19**, 61–83,
782 doi:10.1007/s00382-001-0209-5.

783 Guyard, H., E. Chapron, G. St-Onge, and J. Labrie, 2013: Late-Holocene NAO and oceanic
784 forcing on high-altitude proglacial sedimentation (Lake Bramant, Western French Alps).
785 *The Holocene*, **23**, 1163–1172, doi:10.1177/0959683613483616.
786 http://hol.sagepub.com/content/23/8/1163.abstract.

787 Haarsma, R. J., F. M. Selten and S. S. Drijfhout (2015) Decelerating Atlantic meridional
788 overturning circulation main cause of future west European summer atmospheric
789 circulation changes. *Environmental Research Letters*, **10** (9), doi:10.1088/1748-
790 9326/10/9/094007.

791 Harrison, S. P., P. J. Bartlein, K. Izumi, G. Li, J. Annan, J. Hargreaves, P. Braconnot, and M.
792 Kageyama, 2015: Evaluation of CMIP5 palaeo-simulations to improve climate
793 projections. *Nat. Clim. Chang.*, **5**, 735–743, doi:10.1038/nclimate2649.
794 http://www.nature.com/doifinder/10.1038/nclimate2649.

795 Hawkins, E., and R. Sutton, 2009: The potential to narrow uncertainty in regional climate
796 predictions. *Bull. Am. Meteorol. Soc.*, **90**, 1095–1107, doi:10.1175/2009BAMS2607.1.

797 Huck, T., A. De Colin Verdière, P. Estrade, and R. Schopp, 2008: Low-frequency variations
798 of the large-scale ocean circulation and heat transport in the North Atlantic from 1955-
799 1998 in situ temperature and salinity data. *Geophys. Res. Lett.*, **35**, 1–5,
800 doi:10.1029/2008GL035635.

801 Hurrell, J. W., 1995: Decadal Trends in the North Atlantic Oscillation : Regional
802 Temperatures and Precipitation. Science Vol. 269, No. 5224, pp. 676-679.

803 Hurrell, J. W., and C. Deser, 2010: North Atlantic climate variability: The role of the North
804 Atlantic Oscillation. *J. Mar. Syst.*, **79**, 231–244, doi:10.1016/j.jmarsys.2009.11.002.

805 IPCC Working Group 1, I., and Coauthors, 2013: IPCC, 2013: Climate Change 2013: The
806 Physical Science Basis. Contribution of Working Group I to the Fifth Assessment Report
807 of the Intergovernmental Panel on Climate Change. *IPCC*, **AR5**, 1535.

808 Jackson, L. C. et al. (2015) Global and European climate impacts of a slowdown of the
809 AMOC in a high resolution GCM. *Climate Dynamics*, **45** (11-12), 3299-3316,
810 doi:10.1007/s00382-015-2540-2.

811 Joshi et al. (2008) Mechanisms for the land/sea warming contrast exhibited by simulations of
812 climate change. *Climate Dynamics* 30: 455. https://doi.org/10.1007/s00382-007-0306-1

813 Jungclaus, J. H., and Coauthors, 2013: Characteristics of the ocean simulations in the Max
814 Planck Institute Ocean Model (MPIOM) the ocean component of the MPI-Earth system
815 model. **5**, 422–446, doi:10.1002/jame.20023.

816 Kissel, C., A. Van Toer, C. Laj, E. Cortijo, and E. Michel, 2013: Variations in the strength of
817 the North Atlantic bottom water during Holocene. *Earth Planet. Sci. Lett.*, **369–370**,
818 248–259, doi:10.1016/j.epsl.2013.03.042. http://dx.doi.org/10.1016/j.epsl.2013.03.042.

819 Klein, F., H. Goosse, A. Mairesse, A. De Vernal, and P. L. Pasteur, 2014: Model – data
820 comparison and data assimilation of mid-Holocene Arctic sea ice concentration. 1145–
821 1163, doi:10.5194/cp-10-1145-2014.

822 Li, L., and Coauthors, 2013: The flexible global ocean-atmosphere-land system model, Grid-
823 point Version 2: FGOALS-g2. *Adv. Atmos. Sci.*, **30**, 543–560, doi:10.1007/s00376-012-
824 2140-6.

825 Masson, V., R. Cheddadi, P. Braconnot, S. Joussaume, and D. Texier, 1999: Mid-Holocene
826 climate in Europe: What can we infer from PMIP model-data comparisons? *Clim. Dyn.*,
827 **15**, 163–182, doi:10.1007/s003820050275.

828 Massonnet F., T. Fichefet, H. Goosse, C. M. Bitz, G. Philippon-Berthier, M. M. Holland, P. -
829 Y. Barriat (2012) Constraining projections of summer Arctic sea ice. *The Cryosphere* 6,
830 1383-1394.

831 Mauri, A., B. A. S. Davis, P. M. Collins, and J. O. Kaplan, 2014: The influence of
832 atmospheric circulation on the mid-Holocene climate of Europe: A data-model
833 comparison. *Clim. Past*, **10**, 1925–1938, doi:10.5194/cp-10-1925-2014.

834 McCarthy, G. D. et al., 2015: Measuring the Atlantic Meridional Overturning Circulation at
835 26 degrees N. *Progress in Oceanography*, **130**, 91-111,
836 doi:10.1016/j.pocean.2014.10.006.

837 Otto, J., T. Raddatz, and M. Claussen, 2009: Climate variability-induced uncertainty in mid-
838 Holocene atmosphere-ocean-vegetation feedbacks. *Geophys. Res. Lett.*, **36**, 1–5,
839 doi:10.1029/2009GL041457.

840 Ritz, S. P., T. F. Stocker, J. O. Grimalt, L. Menviel, and A. Timmermann, 2013: Estimated
841 strength of the Atlantic overturning circulation during the last deglaciation. *Nat. Geosci.*,
842 **6**, 208–212, doi:10.1038/ngeo1723. http://www.nature.com/doifinder/10.1038/ngeo1723.

843 Rotstayn, L. D., S. J. Jeffrey, M. A. Collier, S. M. Dravitzki, A. C. Hirst, J. I. Syktus, and K.
844 K. Wong, 2012: and Physics Aerosol- and greenhouse gas-induced changes in summer
845 rainfall and circulation in the Australasian region : a study using single-forcing climate
846 simulations. 6377–6404, doi:10.5194/acp-12-6377-2012.

847 Saint-Lu, M., P. Braconnot, J. Leloup, and O. Marti, 2016: The role of El Ni??o in the global
848 energy redistribution: a case study in the mid-Holocene. *Clim. Dyn.*, 1–18,
849 doi:10.1007/s00382-016-3266-5.

850 Scaife A., Smith, D. (2018) A signal-to-noise paradox in climate science. Climate and
851 Atmospheric Science 1:28 ; doi:10.1038/s41612-018-0038-4

852 Schmidt, G. A., and Coauthors, 2006: Present-Day Atmospheric Simulations Using GISS
853 ModelE: Comparison to In Situ, Satellite, and Reanalysis Data. *J. Clim.*, **19**, 153–192,
854 doi:10.1175/JCLI3612.1. http://journals.ametsoc.org/doi/abs/10.1175/JCLI3612.1.

855 Schmidt, G. A., and Coauthors, 2014: Using palaeo-climate comparisons to constrain future
856 projections in CMIP5. *Clim. Past*, **10**, 221–250, doi:10.5194/cp-10-221-2014.

857 Shi, X., and G. Lohmann (2016), Simulated response of the mid- Holocene Atlantic
858 meridional overturning circulation in ECHAM6-FESOM/MPIOM, J. Geophys. Res.
859 Oceans, 121, 6444–6469, doi:10.1002/ 2015JC011584.

860 Swingedouw, D., P. Braconnot, and O. Marti, 2006: Sensitivity of the Atlantic Meridional
861 Overturning Circulation to the melting from northern glaciers in climate change
862 experiments. *Geophys. Res. Lett.*, **33**.

863 ——, J. Mignot, P. Braconnot, E. Mosquet, M. Kageyama, and R. Alkama, 2009: Impact of
864 freshwater release in the north atlantic under different climate conditions in an OAGCM.
865 *J. Clim.*, **22**, 6377–6403, doi:10.1175/2009JCLI3028.1.

866 Swingedouw, D., C. B. Rodehacke, S. M. Olsen, M. Menary, Y. Gao, U. Mikolajewicz, and J.
867 Mignot, 2015a: On the reduced sensitivity of the Atlantic overturning to Greenland ice
868 sheet melting in projections: a multi-model assessment. *Clim. Dyn.*, **44**, 3261–3279,
869 doi:10.1007/s00382-014-2270-x. http://dx.doi.org/10.1007/s00382-014-2270-x.

870 Swingedouw, D., and Coauthors, 2015b: Bidecadal North Atlantic ocean circulation

variability controlled by timing of volcanic eruptions. *Nat. Commun.*, 6, pages: 6545.

Voldoire, A., and Coauthors, 2013: The CNRM-CM5.1 global climate model: Description and basic evaluation. *Clim. Dyn.*, **40**, 2091–2121, doi:10.1007/s00382-011-1259-y.

Watanabe, M., M. Chikira, Y. Imada, and M. Kimoto, 2011: Convective control of ENSO simulated in MIROC. *J. Clim.*, **24**, 543–562, doi:10.1175/2010JCLI3878.1.

Weaver, A. J., and Coauthors, 2012: Stability of the Atlantic meridional overturning circulation: A model intercomparison. *Geophys. Res. Lett.*, **39**, 1–7, doi:10.1029/2012GL053763.

Wohlfahrt, J., S. P. Harrison, P. Braconnot, C. D. Hewitt, A. Kitoh, U. Mikolajewicz, B. L. Otto-Bliesner, and S. L. Weber, 2008: Evaluation of coupled ocean-atmosphere simulations of the mid-Holocene using palaeovegetation data from the northern hemisphere extratropics. *Clim. Dyn.*, **31**, 871–890, doi:10.1007/s00382-008-0415-5.

Xin, X., L. Zhang, J. Zhang, T. Wu, and Y. Fang, 2013: Climate Change Projections over East Asia with BCC _ CSM1 . 1 Climate Model under RCP Scenarios. **91**, 413–429, doi:10.2151/jmsj.2013-401.

Yukimoto, S., Y. Adachi, M. Hosaka, and T. Sakami, 2012: A New Global Climate Model of the Meteorological Research Institute : MRI-CGCM3 — Model Description and Basic Performance —. **90**, doi:10.2151/jmsj.2012-A02.